Transition metal-doped TiO_2 and ZnO—present status of the field

2005 J. Phys.: Condens. Matter 17 R657

(http://iopscience.iop.org/0953-8984/17/27/R01)

INSTITUTE OF PHYSICS PUBLISHING JOURNAL OF PHYSICS: CONDENSED MATTER

J. Phys.: Condens. Matter **17** (2005) R657–R689 doi:10.1088/0953-8984/17/27/R01

TOPICAL REVIEW

Transition metal-doped TiO_2 and ZnO—present status of the field

Rebecca Janisch[1,2], **Priya Gopal**[1] **and Nicola A Spaldin**[1]

[1] Materials Department, University of California Santa Barbara, CA, USA
[2] Fakultät für Elektrotechnik und Informationstechnik, Technische Universität Chemnitz, Germany

Received 6 April 2005
Published 24 June 2005
Online at stacks.iop.org/JPhysCM/17/R657

Abstract

There has been considerable recent interest in the design of diluted magnetic semiconductors, with a particular focus on the exploration of different semiconductor hosts. Among these, the oxide-based diluted magnetic semiconductors are attracting increasing attention, following reports of room temperature ferromagnetism in anatase TiO_2 and wurtzite ZnO doped with a range of transition metal ions. In this review we summarize the current status of oxide-based diluted magnetic semiconductors, and discuss the influence of growth method, substrate choice, and temperature on the microstructure and subsequent magnetic properties of thin films. We outline the experimental conditions that promote large magnetization and high ferromagnetic Curie temperature. Finally, we review the proposed mechanisms for the experimentally observed ferromagnetism and compare the predictions to the range of available data.

(Some figures in this article are in colour only in the electronic version)

Contents

1. Introduction

The emerging research area known as 'spintronics' seeks to extend the properties and applications of established electronic devices by making use of the spin of electrons in addition to their charge [1]. In particular, the long spin coherence length of electrons suggests that the movement of spin, like the flow of charge, could be used to convey information. Such spin-polarized electronic devices could be much smaller, consume less electricity, and be more effective for certain kinds of computations than today's systems [2], which are based on electron charge only. In addition to its potential utility, the study of spin-polarized transport is revealing new and fascinating fundamental physics [1].

Existing magnetic devices, such as read heads for magnetic data storage technology which exploit the giant magnetoresistance effect, are based largely on ferromagnetic metals. The development of magnetic semiconductors, which would allow signal amplification and would be compatible with standard semiconductor growth techniques, would open new possibilities. In fact magnetism and semiconducting properties are known to coexist in some ferromagnetic semiconductors, such as europium chalcogenides [3] and ferrimagnetic or ferromagnetic semiconducting spinels [4, 5], that have a periodic array of magnetic elements, shown schematically in figure 1(A). Often such magnetic semiconductors are difficult to grow, are incompatible with common semiconductor materials such as Si or GaAs, and have low Curie temperatures, typically well below 100 K. An alternative is offered by the so-called *diluted magnetic semiconductors* (DMS) in which non-magnetic semiconductors (figure 1(B)) are doped with magnetic atoms (figure 1(C)).

There has been considerable recent progress in the design of DMS, and a number of different semiconductor hosts have been explored. DMS based on II–VI semiconductors such as CdTe or ZnSe are able to accommodate large quantities of magnetic dopants, since the valence of the cation (2+) matches that of common magnetic ions, such as Mn. They have been studied extensively for their interesting magneto-optical properties (see e.g. [6]). However, the magnetic interaction in II–VI semiconductors is dominated by the *anti*ferromagnetic exchange among the Mn spins [6] and it has proved difficult to create p- or n-type carriers to mediate *ferro*magnetic interactions [7, 8]. In fact, ferromagnetism has so far only been achieved at low temperatures ($T \leqslant 4$ K), which makes II–VI DMS unattractive for practical electronic applications. More promising are DMS based on III–V semiconductors such as GaAs or InAs. When divalent transition metal ions substitute for trivalent cations in a III–V host, holes are

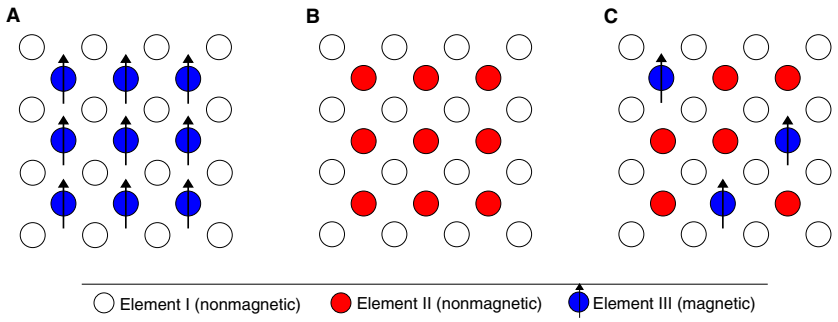

Figure 1. Schematic representation of (A) a magnetic semiconductor, (B) a non-magnetic semiconductor, and (C) a diluted magnetic semiconductor. In the style of [8].

also introduced, which are believed to mediate the observed ferromagnetic ordering in these systems. The Curie temperatures (T_Cs) are generally higher than those in II–VI DMS (up to around 100 K), but have not reached the room temperature values that are desirable for applications [8, 9].

Recently several oxide-based DMS have been reported to be robust, room temperature ferromagnets. In particular the Co-doped TiO_2 system, first reported to be ferromagnetic by Matsumoto *et al* [10], has received much attention. Subsequent experimental studies suggest T_Cs up to ∼650 K, although a large range of T_Cs and magnetizations have been reported, depending on the preparation conditions and the distribution and concentration of Co. A consensus on the origin of the ferromagnetic coupling has not yet been reached, and in some cases it probably results from the presence of Co clusters ($T_C \approx 1180$ K). Work on the ZnO-based system was motivated by a prediction of room temperature ferromagnetism in p-type Mn-doped ZnO [11]. Following this prediction, many researchers have grown ZnO doped with the entire series of 3d transition metal ions; while some of them report high room temperature ferromagnetism [12–14], others report observation of either a spin-glass or a paramagnetic behaviour in their samples [15].

The purpose of this review is to extract trends from the range of experimentally observed and computationally predicted properties of Co-doped TiO_2 [16–45], and Mn- and Co-doped ZnO [15, 46–60] to shed some light on the origin and optimization of the magnetic properties. We will also summarize and discuss the effect of other transition metal dopants in both oxides, including V [48, 49, 61–63], Cr [47, 49, 64–67], Mn [45, 68, 69], Fe [15, 41, 45, 47–49, 68–76], and Ni [41, 45, 47–49, 73–75, 77]. Our goal is to outline the similarities of and differences between the magnetisms in ZnO- and TiO_2-based systems, and to evaluate the theoretical models for both. In particular we will answer the following questions:

- Which growth techniques and growth parameters lead to which microstructures?
- Is there a relationship between the microstructure and the magnetic properties?
- What is the origin of the ferromagnetism/the nature of the magnetic coupling?

The remainder of this review is organized as follows. In the next section we summarize the theoretical models that have been proposed for explaining ferromagnetism in diluted magnetic semiconductors in general, and in oxide-based DMS in particular. In sections 3 and 4 we describe the experimental results for TiO_2-based and ZnO-based DMS respectively. Section 5 contains the theoretical results for both systems, and we summarize in section 6.

2. Origins of (ferro)magnetism in DMS

In this section we describe the models that are most commonly used to describe the magnetic interactions in diluted magnetic semiconductors. Some, such as the double-exchange interaction, exclusively promote ferromagnetism, whereas most can result in either ferromagnetic or antiferromagnetic interactions, depending on the details of the chemical bonding, geometry, defect structure, and/or carrier concentration.

2.1. Exchange in insulators: direct and superexchange

(a) Direct exchange. The direct exchange interaction coupling the spins, $\mathbf{s}_i$, of *localized* electrons in insulators can be described by the Heisenberg Hamiltonian [78, 79]:

$$H_{\mathrm{ex}} = -\sum_{ij} J_{ij}\mathbf{s}_i \cdot \mathbf{s}_j. \tag{1}$$

If the two states of interest coupled by the exchange integral J_{ij} are electronic states in a free atom, then J_{ij} tends to be positive and the spins align parallel, as reflected in Hund's rules. If the interaction takes place between electrons localized on different neighbouring atoms, J_{ij} tends to be negative; this corresponds to the situation in which two electrons align antiparallel to form a bonding state. In a solid with unpaired electrons, the sign of J_{ij} may in principle be either positive or negative, but typically the negative part dominates, leading to antiferromagnetic alignment of neighbouring spins.

(b) Superexchange. In many transition metal oxides and related materials, magnetic interactions between the transition metal ions are mediated by the intermediate anions; such magnetic coupling is known as superexchange. Superexchange can still be described by a Heisenberg Hamiltonian, in which the sign of J_{ij} is determined by the metal–oxygen–metal bond angle and the d electron configuration on the transition metal. These dependences are summarized in the semi-empirical Goodenough–Kanamori–Anderson rules (e.g. [78]).

2.2. Carrier-mediated exchange

The term 'carrier-mediated exchange' refers to interactions between localized magnetic moments that are mediated by free carriers in the system. Below we describe three limiting cases: the RKKY interaction, Zener carrier-mediated exchange, and Zener double exchange. Most practical systems exhibit features of two or all of the models.

The Rudermann–Kittel–Kasuya–Yosida (RKKY) interaction (see e.g. [80]) formally describes the magnetic exchange between a single localized magnetic moment and a free electron gas. This system can be treated exactly quantum mechanically, and the sign of the exchange interaction, J, can be shown to oscillate with the distance from the localized moment, R, and with the density of electrons in the free electron gas:

$$J(R) = \frac{m^\star k_{\mathrm{F}}^4}{\hbar^2} F(2k_{\mathrm{F}}R) \tag{2}$$

where $m^\star$ is the effective mass and k_{F} the Fermi wavevector of the electron gas. The oscillating function

$$F(x) = \frac{x\cos x - \sin x}{x^4} \tag{3}$$

is plotted in figure 2.

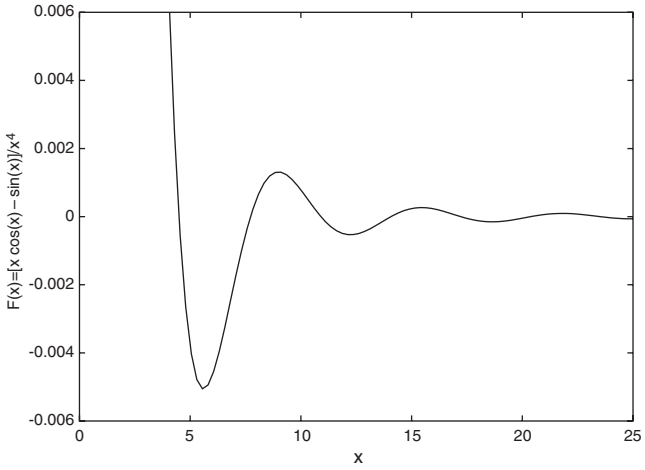

Figure 2. The oscillatory part of the RKKY interaction energy. x is proportional to the product of the Fermi wavevector and the distance from the localized moment.

In systems with both local magnetic moments and itinerant carriers (as in a doped extrinsic DMS) the carriers can mediate a ferromagnetic interaction between the local moments; so-called Zener carrier-mediated exchange [81, 82]. The ferromagnetic ordering is driven by the lowering of the carriers' energy due to redistribution between spin subbands split apart by the exchange interaction.

Finally, the Zener double-exchange model was first proposed [83] to explain the experimentally observed ferromagnetism in the doped perovskite structure manganites, $La_{1-x}A_xMnO_3$, with A = Ca, Sr, or Ba. At intermediate values of $0 < x < 1$ both Mn^{4+} (with three 3d electrons) and Mn^{3+} (with four 3d electrons) are present. The kinetic energy of the system is lowered if the magnetic moments align parallel, since parallel alignment allows electron transfer from Mn^{3+} to Mn^{4+}. This indirect coupling is mediated by the oxygen atoms between neighbouring Mn^{3+} and Mn^{4+} ions, but is distinguished from superexchange by the involvement of carriers.

2.3. Bound magnetic polarons

The concept of bound magnetic polarons (BMPs) in connection with magnetic semiconductors was first introduced to explain the low temperature metal–insulator transition in oxygen-deficient EuO [84]. In the BMP model, oxygen vacancies act both as electron donors, and as electron traps which can bind the electrons and maintain insulating behaviour. Each trapped electron couples the local moments of the host lattice that lie within its orbit ferromagnetically, leading to a bound polaron with a large net magnetic moment. If neighbouring polarons do not interact strongly, a paramagnetic, insulating phase results. However, for certain polaron–polaron distances and combinations of electron–electron and electron–local moment exchange constants, the polarons may couple in a ferromagnetic fashion [85, 86]. It is difficult to make any quantitative prediction, but the critical distance *above* which the exchange between two BMPs becomes ferromagnetic is typically of the order of a few Bohr radii [86]. The amplitude of the exchange interaction then drops off rapidly with distance. Above some critical electron density, the attractive potential of the vacancy is screened, the donor electrons become unbound, and the system metallic (analogously to a Mott insulator–metal transition) [87] and, depending on

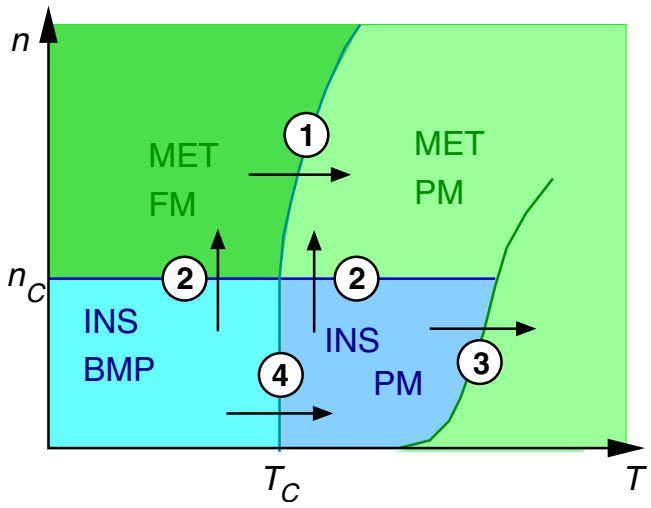

Figure 3. Schematic phase diagram of an oxygen-deficient semiconductor, doped with magnetic impurities. Shown are the different phases as functions of carrier density n and temperature T. The bound magnetic polarons in the BMP phase *can* couple ferromagnetically. The marked transitions are: (1) the FM–PM transition in the metallic phase at T_C, (2) insulator–metal transitions as vacancies are screened for $n \geqslant n_C$, (3) the insulator–metal transition as electrons become thermally excited into the conduction band, and (4) transition from bound magnetic polarons to atomic paramagnetically ordered spins.

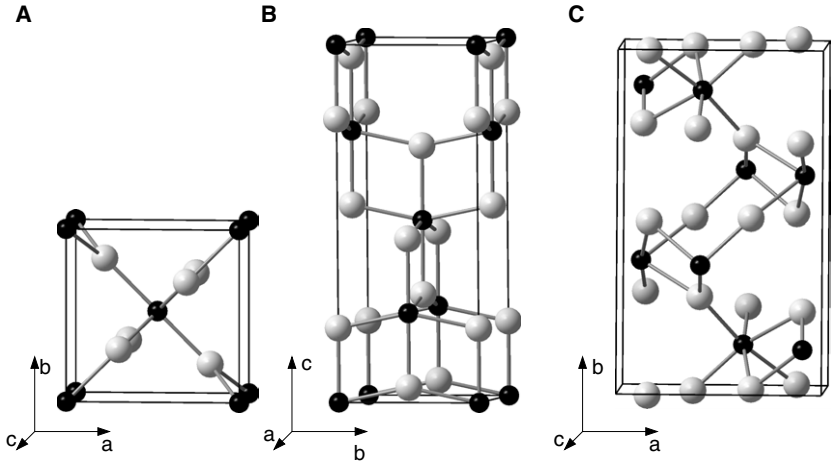

Figure 4. Different polymorphs of TiO_2: (A) rutile, (B) anatase, and (C) brookite.

the temperature, either paramagnetic or ferromagnetic. A schematic diagram of the theoretical BMP phase diagram is shown in figure 3.

3. TiO_2-based DMS: experimental work

3.1. Pure titania

Pure TiO_2 has many polymorphs, of which three, rutile, anatase, and brookite, occur in nature. Unit cells of the structures are shown in figure 4. The relative stability of rutile and anatase

Table 1. Examples of measured [165] and calculated (using density functional theory within the local density approximation) [166] lattice parameters of anatase TiO_2. For a recent compilation see e.g. [88].

	Experiment	Calculation
a (Å)	3.784	3.760
c (Å)	9.515	9.454
c/a	2.515	2.514
u	0.208	0.207

at ambient conditions is a controversial topic in the literature, both from the experimental and theoretical points of view [88–91]. Rutile is thought to be the most stable configuration; however, the reported enthalpies of transformation for TiO_2 polymorphs range from -11.67 to $+8.37$ kJ mol^{-1} for the rutile–anatase transformation (compiled e.g. in [90]).

All of the polymorphs are wide band gap semiconductors, transparent in the visible region, and with a high refractive index. Traditionally the rutile phase has been the most extensively investigated one, experimentally as well as theoretically, the former due to the availability of good single crystals for characterization and the latter because of the comparatively simple crystal structure. Recently, however, experimental investigations have also focused on the anatase phase, because of its promising efficiency for photoelectrochemical use [92]. Representative examples of measured and calculated (using density functional theory within the local density approximation) lattice parameters of anatase are shown in table 1.

3.2. Co-doped TiO_2: growth and characterization techniques

Co-doped TiO_2 has been grown using a wide variety of thin film growth methods, including laser molecular beam epitaxy (LMBE; used by [16, 17, 93]), oxygen plasma assisted MBE (OPA-MBE; see [18–20]), and combinatorial LMBE (employed by [10, 21], described in [94]); as well as pulsed laser deposition (PLD; as used by [22–24, 95]), reactive co-sputtering (of Ti and Co; e.g. done by [25]), and magnetron sputtering [26, 27][3]. In addition, a range of growth conditions and film substrates have been explored. In many cases, since thin film crystal growth happens far from thermal equilibrium, it has been possible to obtain DMS containing magnetic ion concentrations that exceed thermal equilibrium solubility limits. TiO_2 in the rutile phase, which is available in single-crystalline form, has sometimes been doped by means of ion implantation, for example in [32] and [39].

The resulting TiO_2 thin films have been characterized by x-ray diffraction (XRD) to determine the crystal structure, and often by conventional as well as high resolution (HR) transmission electron microscopy (TEM), to reveal the presence of defects such as dislocations and grain boundaries, as well as the occurrence of precipitates and metallic Co particles. X-ray photoelectron spectroscopy (XPS), which probes the (occupied) electronic core states of an atom by knocking out an inner electron, has been used to identify the oxidation state and bonding environment of Co ions. The unoccupied electronic structure, and in turn the chemical environment of atoms in the solid, has been probed using x-ray absorption spectroscopy (XAS), in particular to investigate substrate surfaces. Electron energy-loss spectroscopy (EELS) has also been used to probe the electronic structure and to determine the oxidation state of Co in TiO_2 by comparing the spectra to those of well-known reference compounds. The combination of quantitative and/or spatially resolved XAS, XPS, or EELS analyses has provided information about the Co content and distribution in the various samples.

[3] For an introduction to the growth of thin films, see e.g. [96, 97].

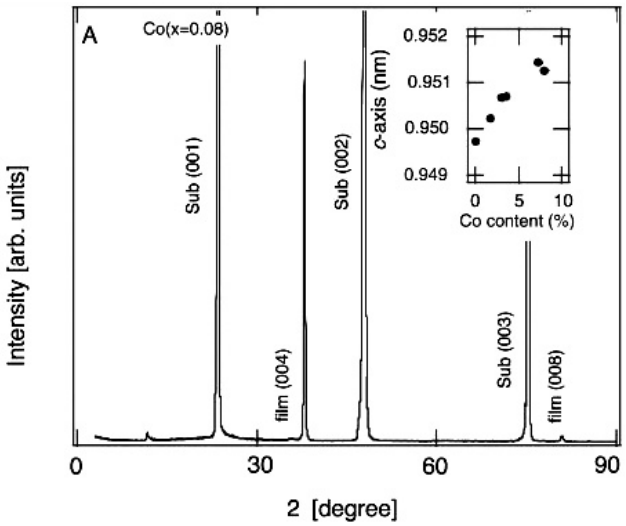

Figure 5. X-ray diffraction peaks of a TiO_2 film grown on $SrTiO_3$. Reprinted with permission from [10]. Copyright 2005 AAAS.

The magnetic properties of the thin films have been investigated using superconducting quantum interference devices (SQUIDs), which can detect weak fields and are useful for determining the saturation magnetization and (in scanning mode) for showing magnetic domain structures (as e.g. in [10]). Optical magnetic circular dichroism (O-MCD) spectra as well as measurements of the anomalous Hall effect have been used to verify the occurrence of intrinsic ferromagnetism in DMS and relate it to the carrier concentration in the samples. (For an overview of TEM techniques, as well as the spectroscopic and magnetic characterization methods mentioned above, see e.g. [98–100].)

3.3. Co-doped TiO_2: first observations

The earliest observation of room temperature ferromagnetism in Co-doped TiO_2 was reported by Matsumoto *et al* [10], who produced $Ti_{1-x}Co_xO_2$ films ($0 \leqslant x \leqslant 0.08$) on $LaAlO_3$(001) and $SrTiO_3$(001) by combinatorial laser molecular beam epitaxy (MBE) at oxygen partial pressures of 10^{-6}–10^{-5} Torr and temperatures of 680–720 °C. X-ray diffraction (XRD) patterns (figure 5) showed the films to be of the anatase structure.

The change in the lattice constant with Co concentration followed Vegard's law and TEM pictures showed no sign of segregation of impurity phases throughout the whole range of Co concentrations ($0 \leqslant x \leqslant 0.08$). Thus it was concluded that Co was homogeneously distributed in the anatase matrix, on substitutional sites.

Magnetic images were taken using a scanning SQUID microscope at 3 K. In all of the Co-doped films, magnetic domain structures of $\approx$20 μm in diameter were observed, suggesting ferromagnetic long range order. The magnitude of the total magnetic moment in the sample increased with increasing Co content. Hysteresis loops, such as that shown in figure 6 for the $x = 0.07$ film on $SrTiO_3$ at room temperature, showed a saturation magnetization corresponding to a magnetic moment of 0.32 μ_B per Co atom. This small magnetic moment suggested that Co was in the low spin state. The resistivity and carrier concentration of

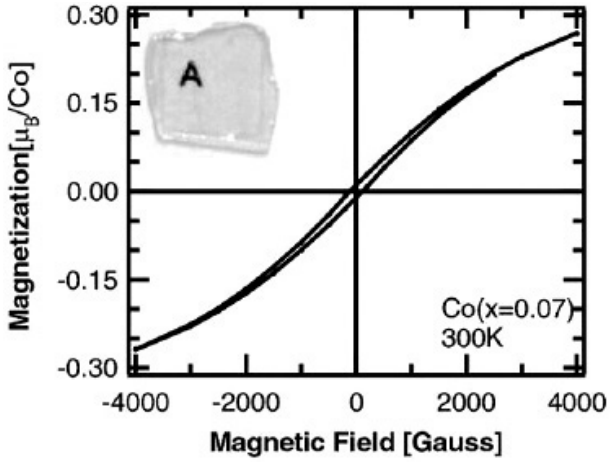

Figure 6. Magnetization versus magnetic field for a $Co_{0.07}Ti_{0.93}O_2$ anatase film on $SrTiO_3$, recorded at 300 K. Reprinted with permission from [10]. Copyright 2005 AAAS.

the films were about 0.1–1 Ω cm and 10^{18} cm^{-3} respectively—typical values for doped semiconductors—almost independent of the Co doping level.

3.4. Co-doped TiO_2: microstructure and magnetism

A flurry of activity followed the initial report of room temperature ferromagnetism in Co-doped TiO_2; however, as yet no simple relationship has been established between the growth method and the microstructure of the film, or the Co distribution in the films. However, it can be said that very low growth rates ($\leqslant 0.03$ Å s^{-1}) lead to epitaxial layer-by-layer growth of TiO_2 [16, 19], whereas high growth rates ($\geqslant 0.4$ Å s^{-1}) produce granular films [25, 26] or precipitation of other phases [19, 23]. Interestingly, the substrate temperature during growth (varying between 600 and 1000 K) does not seem to change the rate dependence of the microstructure.

It is clear that the choice of substrate influences, or even determines, the phase of TiO_2 that is grown. On $LaAlO_3(001)$ only the anatase phase has been grown, independently of the growth method [10, 16, 19, 22, 23, 28, 34, 61, 64, 65, 75], with one exception: the case of Ni-doped TiO_2 [73]. This can be explained by the very small lattice misfit (−0.26%) between this substrate and the TiO_2 anatase phase. On $SrTiO_3(001)$ (in which the anatase lattice mismatch is −3.1%), the anatase phase is again almost always found [10, 18, 22, 28, 32, 38, 73] with one exception reported [26]. Films grown on Si(100) or $Al_2O_3(0001)$ always exhibit the rutile crystal structure [17, 23–25, 28, 33, 66, 70, 74], unless buffer layers are grown in between the substrate and the TiO_2 film [27]. The findings of Suryanarayanan *et al*, however, indicate that the TiO_2 crystal structure on $Al_2O_3(0001)$ can be influenced by the annealing temperature, suggesting a close competition between the stability of competing phases on this substrate [101, 102].

It is difficult to say which factors most strongly affect the dopant distribution in the films. In the case of Co-doped TiO_2, if the samples are granular, or if precipitates are present, Co always shows a tendency to segregate, leading to enriched regions (e.g. [19, 20]). In the epitaxial films, however, metallic Co clusters occur as often as homogeneous distributions of Co atoms, and there is no obvious link to the growth rate or the sample temperature during growth.

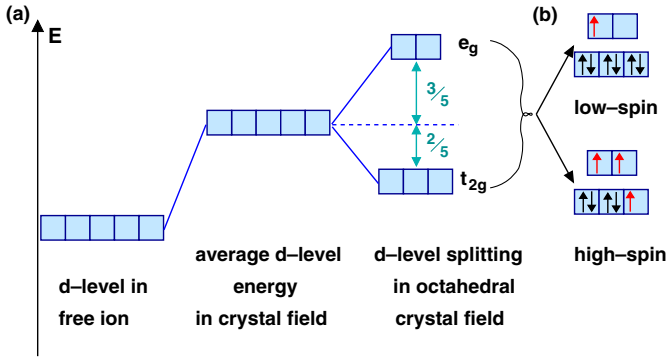

Figure 7. (a) Splitting of d levels in an octahedral crystal field and (b) possible occupation schemes for a Co^{2+} ($3d^7 4s^0$) atom. Unpaired spins are highlighted.

Post-annealing of the samples can lead to redistribution of the Co atoms. Interestingly, in some cases, heating the sample to about 600 K leads to an increased clustering of Co within the film, or precipitation of Co clusters on the film surface [16, 38], while in others, samples which initially show evidence of Co nanoparticles incorporate the Co into the TiO_2 matrix after annealing at 600–670 K [22, 29].

A possible factor influencing the Co distribution could be the presence of oxygen vacancies, as indicated by the work of Kim *et al* [30], who investigated the influence of the oxygen partial pressure (P_{O_2}) during growth on the Co distribution in epitaxial anatase films grown on $SrTiO_3$ by PLD. They found an increasing tendency of Co to cluster, and with it an increasing magnetic moment per Co atom, with decreasing P_{O_2}. Films grown at partial pressures above 10^{-5} Torr did not show any sign of Co inhomogeneity, whereas films grown at 3.3×10^{-7} Torr contained nanoclusters. If a low P_{O_2} during growth increases the number of oxygen vacancies in the sample, then the formation of Co clusters could be explained by the higher mobility of Co in the TiO_2 lattice in these cases.

The charge state of substitutional Co in TiO_2 has been determined to be +2 by several groups, using both x-ray photoelectron spectroscopy and x-ray absorption spectroscopy [16, 18, 19, 93]. However, opinions differ as to whether the ionic ground state (derived from the Co $L_{2,3}$ edge in x-ray absorption spectra) is the Co^{2+} high spin ($3d^7$, $S = 3/2$) [16] or low spin ($3d^7$, $S = 1/2$) [18] state (illustrated schematically in figure 7). The wide range of experimentally determined magnetic moments spans both configurations, and thus the question of the spin state is still to be answered.

The reported room temperature magnetic moments (μ) in Co-doped TiO_2 range from 0.16 μ_B/Co [28] to values as high as $\approx$1.7 μ_B/Co [16, 23, 40], and in some cases even exceed the value for Co metal (which is 1.76 μ_B) [33]. Figure 8 shows the experimental values for μ, related to the thin film crystal structures and the substrates.

In films grown on Si or Al_2O_3 the average magnetic moment per Co atom is below 1 μ_B in all cases. In the samples using $SrTiO_3$ as a substrate the values scatter over more or less the whole range of reported values with a slight accumulation in the lower region. In films grown on $LaAlO_3$, which furthermore are *always* of the anatase structure, most of the values are accumulated in the upper region, i.e. $\mu \geqslant 1.2$ μ_B/Co, but with some scatter between 0.23 and 1.72 μ_B/Co.

In figure 9 we plot the room temperature magnetic moments, measured for films grown on $LaAlO_3$, as a function of the Co concentration x, with the purpose of relating these values to

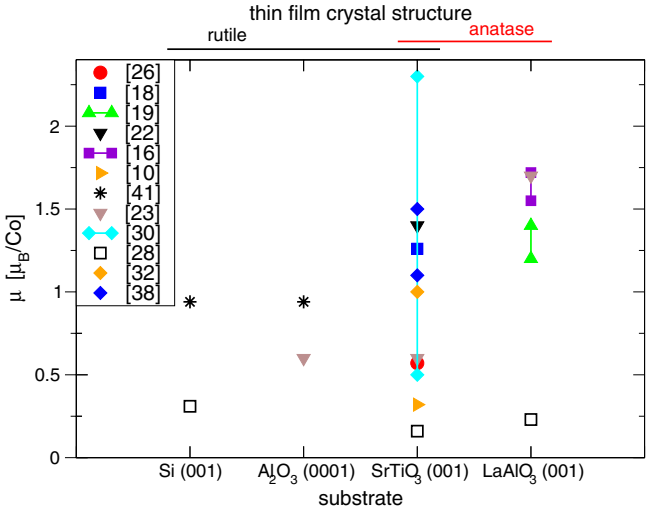

Figure 8. Reported magnetic moments per Co atom for TiO_2 films grown on different substrates. A line between two values measured by the same authors indicates a spread of magnetic moments within this interval. Films on Si and Al_2O_3 persistently grow in the rutile structure, those on Al_2O_3 in the anatase structure. On $SrTiO_3$ both phases can be obtained, depending on the growth method. The magnetic moment per Co atom has been chosen as representative of the magnetic properties of Co-doped TiO_2 because, unlike T_C, it is reported in all the experimental papers, and can be calculated easily by means of electronic structure calculations. It thus allows for direct comparison of theory and experiment.

the reported microstructure. A homogeneous Co distribution throughout the whole epitaxial film has been observed in the $Ti_{1-x}Co_xO_2$ samples with x as small as 0.03 [19], while for $x = 0.1$ the Co forms metallic clusters [16] and in the sample with $x = 0.12$ it segregates towards the surface. The example with $x = 0.07$ is a more exotic one. The film was grown at a very high growth rate (3.3 Å s^{-1}) by PLD and shows an interesting morphology: an epitaxial anatase film which merges into a columnar structure on top of which Co precipitates form as faceted crystals [23]. Thus, here the tendency of Co to segregate probably originates not only from the higher Co concentration, but also from the microstructure.

Avoiding overinterpretation of the data and trends, one can summarize that, for films grown on $LaAlO_3$, a low growth rate and Co concentration lead to epitaxial anatase films with a homogeneous Co distribution and comparatively high room temperature magnetic moments. Higher growth rates and/or higher Co concentrations lead to Co-enriched phases, which can result in high average magnetic moments (probably originating from metallic Co precipitates). This is consistent with the data in figure 10 for films grown on $SrTiO_3$, where one can see that on average the magnetic moment per Co atom decreases with increasing Co concentration. As in the samples grown on $LaAlO_3$, the high value of μ for the low x value of 0.03 comes along with a homogeneous distribution of Co in an epitaxial anatase film [18]. However, no obvious connection between x, μ, and the microstructure (not described in the figure) can be found.

3.5. Origin of ferromagnetism in co-doped TiO_2

Experimental results support two possibilities for the origin of the ferromagnetic ordering of the Co magnetic moments; carrier-mediated exchange (believed to be the mechanism in (Ga, Mn)As [103]) or direct spin–spin interaction. Balagurov *et al* [26], for example, measured

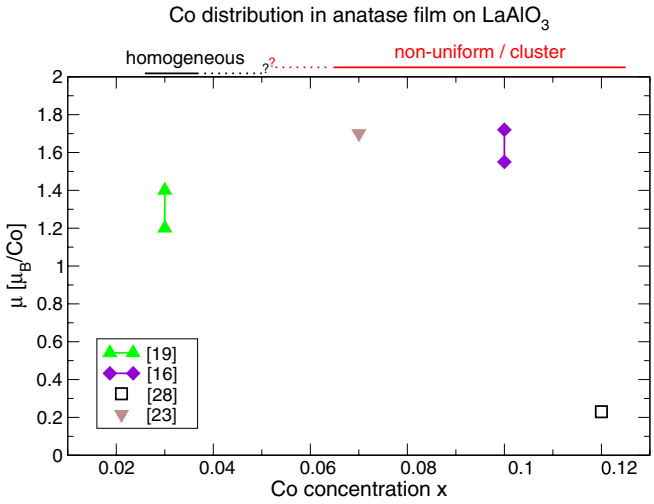

Figure 9. Reported magnetic moments of anatase films grown on $LaAlO_3$, plotted as a function of the Co concentration in the samples. As in figure 8, a line between two values measured by the same authors indicates a spread of magnetic moments within this interval. At low values of x, Co seems to be homogeneously distributed, whereas at higher values Co either tends to segregate, leading to Co-enriched regions, or to precipitate in the form of metal clusters.

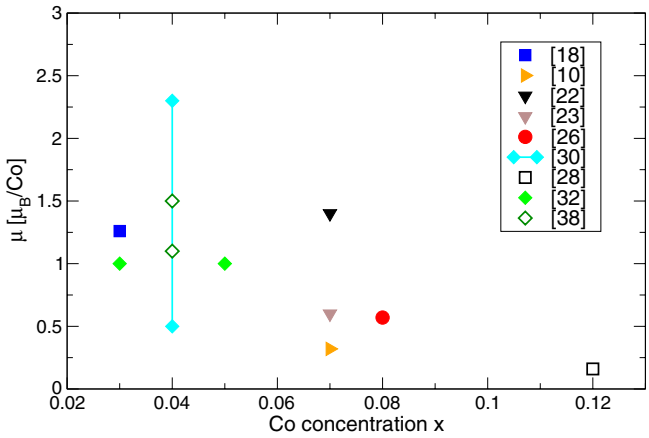

Figure 10. Reported magnetic moments in films grown on $SrTiO_3$, plotted as a function of the Co concentration in the samples.

the magnetism of Co-doped TiO_2 as a function of resistivity. They produced thin films of $Ti_{0.92}Co_{0.08}O_{1-\delta}$ on $SrTiO_3(001)$ by magnetron sputtering of a metal alloy target ($Ti_{0.92}Co_{0.08}$) (with $P_{O_2} = 2 \times 10^{-6} - 2 \times 10^{-4}$ Torr). Samples with low O content exhibited the cubic TiO structure, whereas at higher O concentrations, both the anatase and the rutile phases of TiO_2 were found.

Neither the pure (amorphous) metal alloy $Ti_{0.92}Co_{0.08}$ films nor the insulating $Ti_{0.92}Co_{0.08}O_2$ films exhibited ferromagnetic behaviour. In contrast, magnetic moments of $\mu = 0.87\ \mu_B$/Co and $0.57\ \mu_B$/Co were found in the semiconducting cubic and the anatase $Ti_{0.92}Co_{0.08}O_2$ films respectively (the rutile phase did not occur within the resistivity range

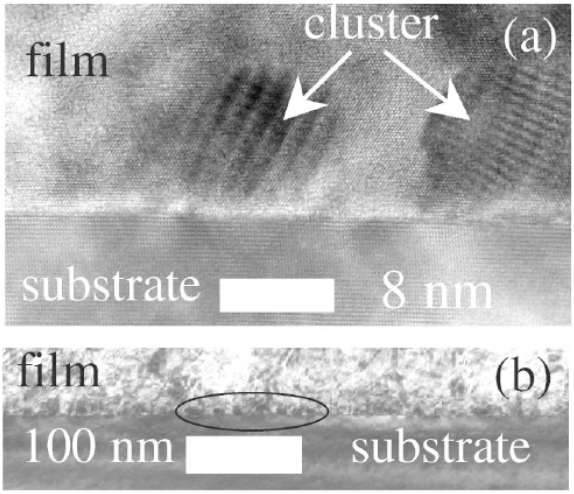

Figure 11. A TEM picture of rutile TiO_2 grown on $LaAlO_3$ with inclusions of Co. From [31]. Copyright (2004) by The American Physical Society.

of interest), *independently* of the resistivity. This behaviour was interpreted as showing that the observed ferromagnetism is based on an exchange, rather than a carrier-mediated mechanism.

Chambers *et al* [19] reached the opposite conclusions. They grew anatase films on $LaAlO_3$ by OPA-MBE at different growth rates and temperatures ranging from 300 to 750 °C, with epitaxy occurring at temperatures above 550 °C. Their undoped TiO_2 films were found to range from being highly conductive n-type semiconductors to being insulators, depending on the Ti/O flux ratio. At low Co concentrations (up to a few atomic per cent (at.%)) their doped samples remained n-type semiconductors with $n_c = (10^{19}–10^{20})$ cm^{-3}. However, at higher Co concentration they became insulating, possibly because the additional Co had a disordering effect on the atomic structure of the films, thus destroying the conduction. Only those samples which were n-type semiconducting (and not insulating) $Ti_{1-x}Co_xO_{2-\delta}$ showed significant magnetism with magnetic moments of 1.2–1.4 μ_B/Co, suggesting that the observed ferromagnetism was carrier mediated.

A connection between carrier density and ferromagnetism, which implies a carrier-mediated exchange mechanism, has also been indicated by measurements of the anomalous Hall effect in Co-doped TiO_2 [17, 24]. Shinde *et al* pointed out, however, that simultaneous occurrence of superparamagnetism and the anomalous Hall effect is possible in Co-doped TiO_2 films [31], and actually demonstrated such a co-occurrence with a Co-doped rutile sample produced by PLD on $LaAlO_3$ [24]. Figure 11 is a TEM picture of their sample, clearly showing Co clusters.

Small single-domain Co particles act, below their blocking temperature, similarly to single localized spins, but with a much larger magnetic moment (hence the expression 'superparamagnetic'). Thus, besides suggesting care when performing Hall measurements, superparamagnetic particles could also be responsible for the occurrence of very high saturation magnetizations. The superparamagnetic size limit for Co metal particles at room temperature is 8 nm diameter, if spherical shape and crystalline anisotropy are assumed (see e.g. [104], p360ff). Particles of this size should be clearly visible in TEM pictures, as demonstrated in [31]. However, smaller particles, which could be missed by TEM imaging, could also

contribute to ferromagnetism, particularly if they were coupled, perhaps by a carrier-mediated exchange mechanism.

3.6. Other transition metal dopants in TiO_2

For transition metal dopants other than Co it is very difficult to derive trends from the available experimental information, since there is much less of it available. Kim *et al* [71] grew Fe-doped rutile under an activated oxygen supply, thus suppressing the occurrence of oxygen vacancies. Nevertheless, Fe was mainly found on the film surface, in the form of antiferromagnetic Fe_3O_4. In reduced rutile, so far no Fe clusters have been reported [70, 72, 74]; however, detailed TEM investigations have only been carried out in one case [70]. A complicating factor as regards a homogeneous spatial distribution of the transition metal dopants is that reduced rutile usually exhibits the Magnéli shear phase Ti_nO_{2n-1}.

Cr as a dopant in TiO_2 so far seems to exhibit no tendency to segregate and/or precipitate in different phases [64–66], up to Cr contents as high as 16 at.% [65].

The magnetic moments determined for Fe substituting for Ti in rutile or anatase TiO_2 range from 0.14 [73] via 0.62 [71] to 2.4 μ_B/Fe [70], suggesting different spin states in the different samples. No relationship between host crystal structure and the magnetic moment is obvious.

Hong *et al* [75] see a continuous trend in their anatase films grown on $LaAlO_3$, doped in turn with V, Cr, Fe, Co, and Ni. Starting with V which exhibits a large magnetic moment (at zero field and low temperatures) around 2.6 μ_B per V, the magnetic moments steadily decrease from Cr to Fe to Co to Ni, with a magnetic moment of about 0.9 μ_B/Ni at $T < 50$ K. This trend is in agreement with the computational results of Errico *et al* [45], who calculated the magnetic moments of Mn, Fe, Co, and Ni in rutile, although the absolute values are not. However, it is inconsistent with the results of another study by Hong *et al* [73] in which they find magnetic moments of 1.3–2.7 μ_B/Ni and 0.14 μ_B/Fe under similar growth conditions.

Cr-doped rutile seems to be a promising, but also puzzling material. Wang *et al* [66] saw the magnetic moment of Cr in Cr-doped reduced rutile grown on Al_2O_3 decrease steadily with increasing Cr concentration: from 2.9 μ_B/Cr at $x = 0.06$ to 0.9 μ_B/Cr at $x = 0.12$. They observed p-type conduction in their samples accompanied by ferromagnetism up to $T \geqslant 400$ K, suggesting hole-mediated, RKKY-like interaction.

In contrast, Droubay *et al* [65] consistently measured $\mu = 0.60 \pm 0.05$ μ_B/Cr in Cr-doped anatase grown on $LaAlO_3$, independently of the Cr concentration, ranging from $x = 0.02$ to 0.16. Their samples ware all insulating and ferromagnetic with $T_C \geqslant 300$ K. Droubay *et al* speculated that this could be due to F-centre exchange, i.e. a form of bound magnetic polarons. So the mechanism of the ferromagnetic interaction seems to be different for different situations in the same material.

4. ZnO-based DMS: experimental work

4.1. Pure ZnO

ZnO is a II–VI semiconductor with a wide band gap of about 3.4 eV. The stable crystal structure (shown in figure 12) of ZnO is wurtzite, in which each atom of zinc is surrounded by four atoms of oxygen in tetrahedral coordination. The wide band gap, which can be tuned over a large energy range by doping with either CdO or MgO [105, 106], means that it is transparent in the visible region. Combined with the high conductivity that can be achieved by doping, this leads to applications in surface acoustic wave devices and transparent conducting electrodes.

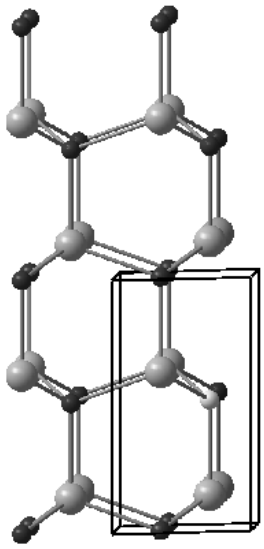

Figure 12. A 2 × 2 × 1 wurtzite supercell of ZnO.

Finally, ZnO is a strong piezoelectric [107], in which the piezoelectric properties can change the characteristics of potential energy barriers at interfaces. The resulting piezoresistance is exploited in metal oxide varistors which can dissipate large amounts of power in short response times and are commonly found as electrical surge protectors [108]. Thus transition metal-doped ZnO has the potential to be a highly multifunctional material with coexisting magnetic, semiconducting, electromechanical, and optical properties.

4.2. Thin films of Mn- and Co-doped ZnO

Incorporating transition metal ions substitutionally in II–VI ZnO should be less difficult than incorporating them in other semiconductor hosts, since the valence of Zn (2+) can be readily adopted by many 3d transition metal ions. This favours substitution of the transition metal ion at the cation site and helps in achieving higher dopant concentrations. It also means that, in a perfectly stoichiometric sample, substitutional Mn introduces a magnetic moment without contributing carriers. Thus, this system can give direct insight into the question of whether the observed ferromagnetism is carrier mediated or not. Most of the initial experimental work on transition metal-doped ZnO has focused on thin films with Mn or Co doping. We review these studies here, and reserve discussion of bulk samples, and other dopants, until later sections.

4.2.1. Mn-doped ZnO. The first experiments on Mn-doped ZnO were performed by Fukumura *et al* [109], who prepared $Zn_{0.64}Mn_{0.36}O$ films using pulsed laser deposition (PLD) on a polished *c*-plane sapphire substrate. The substrate temperature was maintained at 600 °C and the oxygen partial pressure at 10^{-5} Torr. X-ray diffraction measurements showed that the films were of the wurtzite structure without any impurity phases. In addition, electron-probe microanalysis confirmed that the Mn in the film was distributed homogeneously. Magnetic properties were measured using a SQUID magnetometer, which indicated spin-glass behaviour with a freezing temperature of ∼13 K and a large Curie–Weiss temperature suggesting strong *anti*ferromagnetic exchange coupling.

Many experimental studies using a range of growth techniques followed. The most widely reported growth technique is pulsed laser deposition (PLD) [46, 47, 109–112], with the sol–gel method [113], radio-frequency (rf) magnetron sputtering [13, 14, 112, 114, 115], laser molecular beam epitaxy (LMBE) [48], and ion implantation methods [116] also being used. In the following we summarize the dependence of the magnetic behaviour on Mn concentration, substrate choice, growth technique and temperature, and oxygen pressure during growth.

The equilibrium solubility limit of Mn in ZnO has been determined by Bates *et al* to be ∼13% [117]. However, due to the non-equilibrium nature of the different thin film growth techniques, solubilities of up to ∼35% have been routinely obtained, while maintaining the wurtzite structure [48, 109–111, 113, 118]. The concentration of the dopant has a definite influence on the magnetic properties, with more desirable behaviour often obtained at lower concentrations. While ferromagnetic ordering has been reported for Mn concentrations between 2.2 and 30% [12–14, 115, 118], both the magnetic moment per Mn ion and the ferromagnetic T_C seems to decrease with increasing Mn concentration. For example, in [13], the magnetic moment per Mn atom dropped from 4.8 to 0.02 μ_B as the concentration increased from 2.2 to 25 at.%; likewise in [14] the moment dropped from 0.71 to 0.25 emu cm^{-3} when the Mn content increased from 10 to 30 at.%. Only Jung *et al* observed the opposite effect; their saturation magnetization increased from 0.9 to 3.4 emu cm^{-3} for a change in the Mn concentration from 10 to 30% [118]. The ferromagnetic Curie temperature was above room temperature for all concentrations $x \leqslant 5$ at.% [12–14], but usually well below 100 K for higher concentrations [115, 118], again with one exception [14].

Most groups used *c*-plane sapphire as a substrate; this has a low mismatch of only 2% with ZnO [13, 49, 109, 111, 114, 116, 118]. $ScAlMgO_4$ [110], fused quartz [12], MgO [13], Si [112, 113], ZnO [46], and GaAs(001) [14] have also been used. Moodera *et al* [13] compared the dependence of the magnetic behaviour on the use of various substrates, and found ferromagnetic behaviour for films grown on sapphire and MgO(100), but paramagnetic behaviour for films grown on fused quartz and Si. Note, however, that fused quartz was also used by Sharma *et al* [12], who obtained room temperature ferromagnetism, and apart from in the case of the samples of Moodera *et al* [13] no ferromagnetic ordering was found for sapphire [46, 48, 49, 109, 111, 114] or Si [113] substrates. The choice of GaAs as a substrate seemed to [14] enhance the p-type conductivity in ZnO by causing diffusion of As atoms into ZnO and subsequently caused the (Zn, Mn)O films to be ferromagnetic at room temperature.

The substrate temperature during growth and subsequent annealing temperature have a significant influence on the magnetic interactions. Low growth temperatures ($\leqslant$400 °C) seem to be favourable for obtaining ferromagnetic samples [12, 13, 115, 116, 118], which however become paramagnetic when annealed at higher temperatures [12, 13, 113, 118]. In samples that were grown at substrate temperatures above 600 °C no ferromagnetic behaviour was observed [46, 48, 49, 109–111]. Thus low growth and annealing temperatures seem to be favourable for obtaining ferromagnetism in Mn-doped ZnO. No correlation between the magnetic properties and the growth *method* can be extracted, however. For example, samples grown using the PLD technique have shown room temperature ferromagnetism [12] as well as paramagnetism [46–49, 109, 111].

Likewise, ferromagnetic ordering with $T_C \geqslant 300$ K [13, 14] and $T_C = 70$ K [115] as well as paramagnetism [114] have been reported for samples grown by rf magneton sputtering. Similar discrepancies have also been found in films grown using LMBE, where Jung *et al* reported ferromagnetic ordering with a Curie temperature of 45 K [118] while no ferromagnetism was observed in [48].

XRD data indicate a uniform distribution of Mn atoms in ZnO for all of the growth techniques; a typical XRD spectrum is shown in figure 13.

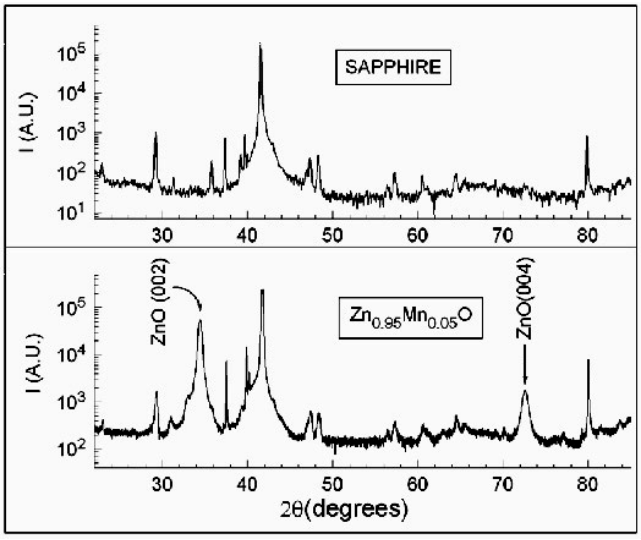

Figure 13. X-ray diffraction pattern for $Zn_{0.95}Mn_{0.05}O$ where the peaks corresponding to the wurtzite structure ZnO are indicated ([13] copyright 2005, the author).

A factor which is commonly believed to influence the magnetic properties is the oxygen partial pressure (P_{O_2}) during growth. A low P_{O_2} favours the formation of oxygen vacancies, which are often assumed to be shallow donors in ZnO, and to dope the system with electrons. However, ferromagnetism has been reported for oxygen pressures of 10^{-5}, 10^{-6}, and 10^{-9} Torr [12, 13, 46, 48, 49, 109–111, 113, 118], with no clear trend in behaviour, suggesting *no* dependence on the presence of oxygen vacancies. It has recently been proposed, however, that oxygen vacancies might stabilize a secondary ferromagnetic phase of ZnMnO [119].

4.2.2. Co-doped ZnO. The first report of ferromagnetism in Co-doped ZnO was made by Ueda *et al* [47], for thin films of $Zn_{1-x}Co_xO$ ($x = 0.05$–0.25) prepared using PLD on sapphire substrates. The x-ray diffraction patterns and the change in lattice parameter as a function of Co concentration are shown in figures 14 and 15. The films were formed at substrate temperatures of 350–600 °C in an oxygen pressure of 2–4 $\times$ 10^{-5} Torr, and with 1 at.% Al added to increase the carrier concentration. Both $Zn_{0.95}Co_{0.05}O$ and $Zn_{0.85}Co_{0.15}O$ showed ferromagnetic hysteresis loops with saturation magnetic moments of 1.8 and 2.0 μ_B respectively, and carrier concentrations of 1.2 $\times$ 10^{18} and 2.9 $\times$ 10^{20} cm^{-3}. The saturation magnetization and Curie temperature increased with increase in the carrier concentration; however, the authors reported that the reproducibility of making samples with ferromagnetic behaviour was less than 10%.

Following these initial reports, thin films of $Zn_{1-x}Co_xO$ were grown by various techniques, including PLD [49–56, 120], rf magnetron co-sputtering [57, 58], sol–gel methods [59], and combinatorial laser molecular beam epitaxy [46, 48]. As in the case of Mn-doped ZnO, the most widely used substrate was sapphire, with one group using hydrothermal ZnO as a substrate for homoepitaxial matching [46].

The thermal solubility limit for Co in ZnO is 10 at.% [117]. Indeed Prellier *et al* [52] observed a plateau in the plot of *c*-lattice parameter versus Co concentration at 10% Co content in PLD-grown films; such a breakdown of Vegard's law marks the solubility limit. Likewise Park *et al* [121] observed the formation of Co nanoclusters for $x \geqslant 12$ at.% in samples grown

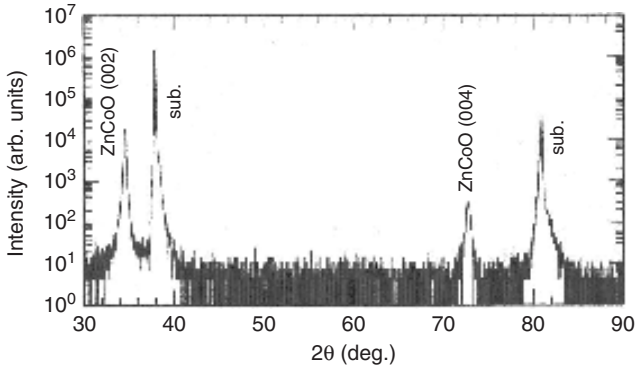

Figure 14. X-ray diffraction pattern of $Zn_{0.85}Co_{0.05}O$. Reprinted with permission from [47]. Copyright 2001, American Institute of Physics.

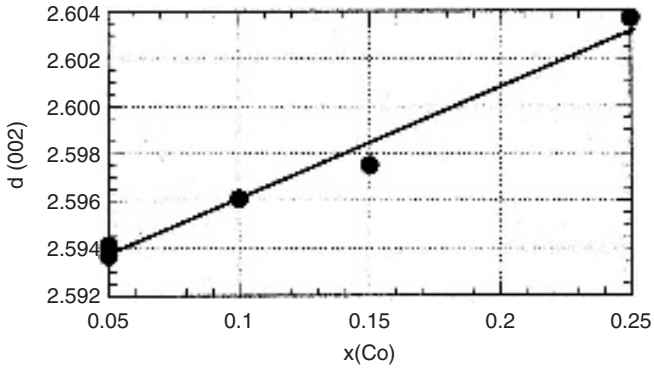

Figure 15. Dependence of the (Zn, Co)O c-axis lattice parameter, $d(002)$, on the cobalt concentration, x(Co). Reprinted with permission from [47]. Copyright 2001, American Institute of Physics.

by sol–gel and rf sputtering techniques. Other groups studied higher doping concentrations: Lee *et al* [59] reported the presence of Co_3O_4 peaks for doping concentrations above 25% using sol–gel methods, Jin *et al* [48] claimed the solubility to be less than 20 at.%, and Ueda *et al* [47] and Kim *et al* [50] found the solubility limit to be less than 50 and 25 at.% respectively in PLD-grown films.

The influences of substrate temperature (up to $\sim$600 °C) and oxygen pressure (varied from 10^{-5} to 5×10^{-5} Torr) were studied in [50], and a schematic diagram showing the conditions for optimal growth is shown in figure 16. Films deposited at lower temperature ($\leqslant$600 °C) and higher oxygen pressures ($\geqslant 10^{-5}$) had a homogeneous distribution of Co, while secondary phases formed at higher temperatures and lower pressures. When the substrate temperature was relatively low ($\leqslant$600 °C), the films were paramagnetic, whereas at higher growth temperatures, mixed phases of wurtzite ZnO with rock-salt CoO and hexagonal Co phases formed and ferromagnetism was observed. For homogeneous films of $Zn_{0.75}Co_{0.25}O$, spin-glass behaviour was obtained.

As regards the values of the saturation magnetization, PLD and rf sputtering growth techniques seem to lead to the best results. However, the measured values for the saturation magnetization spread over a similarly large range to those for Co-doped TiO_2, from 0.56 μ_B/Co [59] to 2.6 μ_B/Co [49]. The variation of the reported measured values of

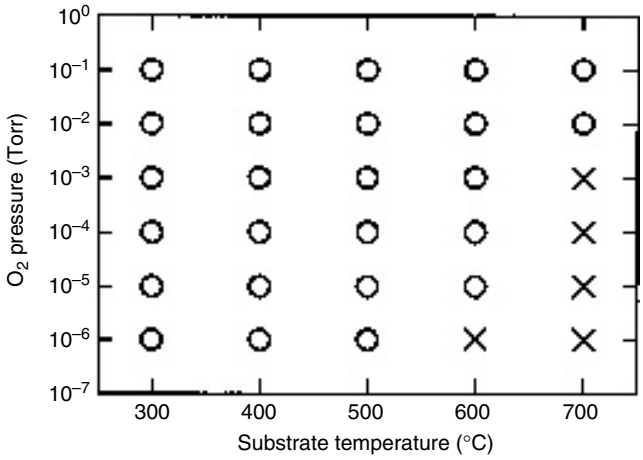

Figure 16. Illustration of the growth phase diagram of $Zn_{0.75}Co_{0.25}O$ films in relation to the two growth parameters (substrate temperature and O_2 pressure). Open circles and crosses denote homogeneous ($Zn_{1-x}Co_xO$) and inhomogeneous ($Zn_{1-x}Co_xO + CoO + Co$) structures respectively. Reprinted with permission from [50]. Copyright 2001, American Institute of Physics.

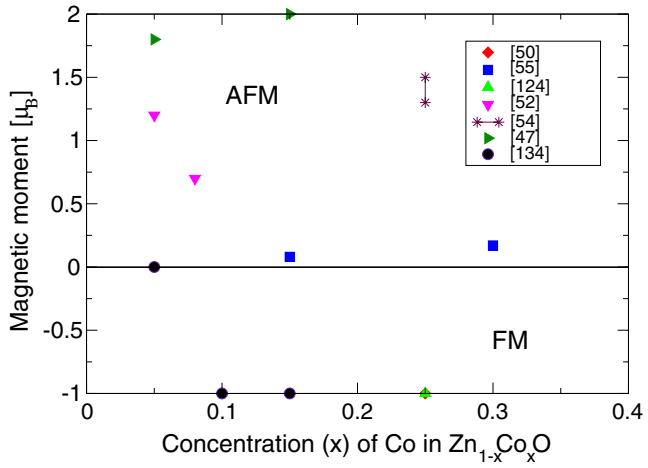

Figure 17. Reported magnetic moment measured in Co-doped ZnO for different dopant concentrations. Reports for both bulk and thin films are plotted.

magnetization for $Zn_{1-x}Co_xO$ samples is plotted in figure 17 as a function of Co concentration, where a negative sign indicates antiferromagnetic, and a positive sign ferromagnetic coupling. As in TiO_2, it is not clear whether Co in ZnO (formally in the oxidation state 2+) is in its low spin ($\mu = 1\ \mu_B$) or high spin ($\mu = 3\ \mu_B$) state. As figure 17 also shows, the influence of Co concentration on the magnetic interactions is also not clear. While some groups report room temperature ferromagnetism for 25 at.% [59] and lower concentrations ($\leqslant$15%) [49, 52, 56, 122] of Co, others report the absence of FM behaviour [48, 50, 121].

4.3. Bulk samples

If the magnetism reported in the Co- and Mn-doped ZnO thin films is intrinsic in nature, one should see similar behaviour in bulk samples, where effects on the microstructure and the

magnetic interaction due to lattice mismatch between substrate and thin film are obviously eliminated.

A few research groups have grown bulk samples (both polycrystalline powders and single crystals) of Co- and Mn-doped ZnO. Growth processes for obtaining polycrystalline samples include precursor decomposition [60, 123], standard solid state reactions [124, 125], diffusion doping of Mn in ZnO tetrapod structures [126], and the high temperature combustion technique [127], while single crystals have been obtained by chemical vapour transport [112], ion implantation [128], and modified melt-growth techniques [129].

The first bulk polycrystalline samples of $Zn_{1-x}Mn_xO$ ($x = 0.05$–0.20) were prepared in air at 1350 °C using a standard solid state reaction technique [125]. The samples were then annealed in an atmosphere of Ar, H_2, or O_2 under 600 bar. X-ray diffraction data showed a small amount of spinel-like $(Mn, Zn)_2O_4$ phase in samples with $x = 0.15$ and 0.20. It was concluded, and subsequently confirmed by other groups, that the solubility limit of Mn was less than 10 at.% [125, 130]. Increasing the Mn concentration gave rise to impurity peaks identified as originating from MnO, $(Mn, Zn)Mn_2O_4$ [130], or spinel-like $ZnMn_2O_4$ [125]. Magnetic susceptibility measurements for $Zn_{0.9}Mn_{0.1}O$ at temperatures of $T = 120$–350 K indicated antiferromagnetic interactions [125].

In samples prepared by low temperature techniques, both ferromagnetic [12, 131, 132] and paramagnetic [60, 123, 129, 130] behaviours have been reported, while samples synthesized at high temperature [112, 125, 133] all showed paramagnetic behaviour. In those samples that initially showed ferromagnetism, the magnetism decayed as a function of the annealing temperature, and all samples annealed above 700 °C became paramagnetic [12, 132]. This leads to the conclusion that higher temperatures, either during growth or during post-annealing, are detrimental as regards ferromagnetic interactions, and does not support the case for intrinsic ferromagnetism in Mn-doped ZnO.

In the case of Co-doped ZnO, no definite conclusions have been reached about the nature of the magnetic interactions. The solubility of Co in ZnO has been determined as being less than 20%, with impurity phases such as CoO and Co_3O_4 forming at higher concentrations [15]. However, Co metal precipitates have formed at only 5 at.% concentration both on annealing [15] and in single crystals [129, 131], and have been proposed as the source of ferromagnetism. In most cases, stoichiometric polycrystalline samples with low Co concentration were paramagnetic [15, 60, 134, 135], with one report of ferromagnetism [136]. In the latter sample, obtained with the solid state reaction method, XRD confirmed that the sample was homogeneous and no impurity phases were found.

4.4. Other dopants in ZnO; V, Cr, Fe, and Ni

In addition to the large number of experiments focused on Co- and Mn-doped ZnO, there have been numerous thin film growth reports for V- [48, 49, 62, 63], Cr- [47, 49, 67], Fe- [47–49, 76], and Ni- [47–49, 77] doped ZnO. A plot of the reported magnetic measurements for the different transition metals, each at a dopant concentration of 5%, is shown in figure 18. V-doped ZnO showed (in some cases) room temperature ferromagnetism with a magnetic moment of 0.5 μ_B. Samples of Ni-doped ZnO prepared by PLD on sapphire showed superparamagnetic behaviour at 300 K, with the ferromagnetic state stabilized by the addition of carriers at 2 K [77]. Venkatesan *et al* found high temperature ferromagnetic ordering with a saturation magnetic moment of 0.8 μ_B for Fe-doped ZnO [49], whereas paramagnetic behaviour was reported by other groups [15, 47, 48].

The possible effects of co-doping, that is simultaneous doping of ZnO with two or more transition metal ions, are interesting. Ferromagnetic transition temperatures as high

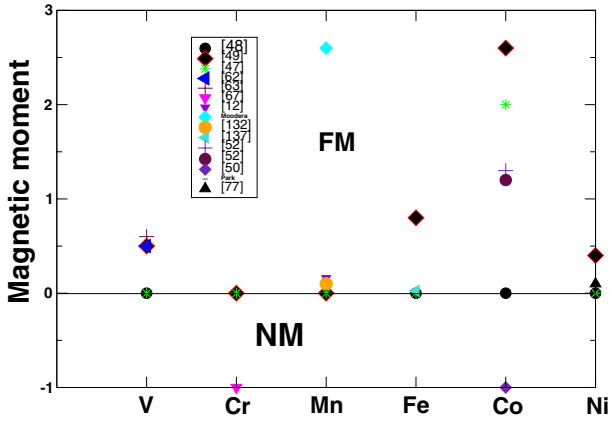

Figure 18. Reported magnetic moments for 5% dopant concentration of the 3d transition metal atoms in ZnO.

as 550 K have been reported for $Zn_{0.94}Fe_{0.05}Cu_{0.01}O$, with a saturation magnetic moment of 0.75 μ_B [137]. Cu is believed to act as an acceptor in the ZnO samples and thus to provide free carriers. Cho *et al* [76] grew thin films of Co–Fe-doped ZnO ($Zn_{0.94}Co_{0.05}Fe_{0.05}O$) by rf magnetron sputtering and observed high temperature ferromagnetism with a magnetic moment of 5.4 emu cm^{-3} (increasing with rapid thermal annealing of the samples to 15 emu cm^{-3}). Lee *et al* fabricated ZnO doped with Cr as well as co-doped with Li and Cr, using the sol–gel method. While the Cr-doped ZnO samples showed paramagnetic behaviour, a clear magnetic hysteresis loop was obtained for the Li–Cr-doped ZnO thin films above 350 K.

4.5. Origin of ferromagnetism in transition metal-doped ZnO

From the broad spread of experimental data it is difficult to draw general conclusions about the nature of magnetic interactions in transition metal-doped ZnO. In Co-doped ZnO, the addition of 1% Al as a dopant, or a decrease in the oxygen partial pressure during growth, seem to increase the carrier concentration and enhance the ferromagnetism [46, 47, 49, 54, 55, 58]. This suggests the presence of carrier-mediated exchange. However, some groups report the observation of FM interactions in the absence of free carriers [46, 52, 56, 59]. Likewise, in Mn-doped ZnO, FM coupling is observed both in the presence [14, 116] and in the absence of carriers [12, 13]. One common feature is that all samples tend to phase segregate at high dopant concentrations and annealing temperatures, and often these second phases are likely to be responsible for the observed ferromagnetism. For example ferromagnetic $Mn_{2-x}Zn_xO_{3-\delta}$ has been proposed as the origin of high temperature ferromagnetism in (Zn, Mn)O [119], and a number of ferromagnetic or ferrimagnetic Co-based phases are known.

5. Computational work

5.1. Electronic structure calculations

The computational results described in this paper were produced using a range of electronic structure implementations, all based on the density functional theory (DFT) of Hohenberg and Kohn [138]. In DFT, the total energy of a many-electron system is described as a functional of the electron density. Expressing the electron density as a sum over one-electron

densities and using the one-electron wavefunctions as variational parameters leads to the Kohn–Sham equations [139], an effective one-electron representation of the many-electron Schrödinger equation, which is formally exact. However, one component of the total energy, the exchange–correlation energy E_{xc}, is unknown within the Kohn–Sham formalism, and must be approximated. The most widely used approximation is the local density approximation (LDA), which assumes that E_{xc} for a single electron at position $\mathbf{r}$ in the real system to be equal to E_{xc} for an electron in an homogeneous, non-interacting electron gas with density equal to the local density $n(\mathbf{r})$. The relaxation of the constraint of an equal occupation of spin-up and spin-down states and the minimization of the total energy with respect to spin occupancy leads to the local spin-density approximation (LSDA) which allows the treatment of magnetic properties (e.g. [140]). Spin–orbit (SO) coupling can be introduced by using a relativistic description, or can be added as a correction.

The LDA has been very successful in predicting many material properties, but also has a few shortcomings: energies of excited states, and in particular band gaps in semiconductors, are systematically underestimated. Furthermore, there is a general tendency to overbinding; thus cohesive energies are often too large, and lattice constants are underestimated (up to 3%). The problems can be particularly acute for magnetic systems, in which the highly localized, spin-polarized electrons are poorly approximated by a free electron gas. In many cases, for example, the LDA predicts a half-metallic, low spin state of magnetic ions, for systems which are experimentally insulating and high spin.

Various 'beyond-LDA' strategies have been developed, among them the addition of a Hubbard correction, U, which takes into account the d–d Coulomb interaction, to the (orbital-independent, one-electron) LDA Hamiltonian (LDA + U [141]), the correction of the spurious self-interaction (SIC) (see [142–145] and references therein) and the application of the generalized gradient approximation (GGA) [146–148], which includes an explicit dependence of E_{xc} on the gradient of the electron density. There are a few cases where e.g. the GGA overcorrects the deficiencies of the LDA, but in general the 'beyond-LDA' methods considerably improve the prediction of electronic energy gaps and magnetic and orbital ordering in systems where electron localization plays a major role.

In addition to a variety of exchange–correlation functionals, there are different possibilities for representing the one-electron wavefunctions in a basis set. We emphasize that these do not represent different physical approximations, but rather different computational implementations, and so, if performed correctly, should all give identical results. The different choices usually fall into one of the following three categories:

- A plane-wave basis in combination with pseudopotentials for describing the interaction between valence electrons and the ionic core.
- Linearized augmented plane waves (LAPWs), i.e. plane waves for the interstitial regions augmented by spherical, atomic-like wavefunctions centred at the atomic sites, or full potential LAPWs (FLAPWs), which differ from LAPWs in that no shape approximations to the effective one-electron potential are made. Similar basis sets are used in the linear muffin-tin orbital (LMTO) methods.
- Linear combinations of atomic orbitals (LCAO).

5.2. *Doped TiO_2*

5.2.1. FM versus AFM and the distribution of the dopant. Park *et al* [41] calculated the properties of Co-doped TiO_2 using the LMTO method, both in the local spin-density approximation and in the LSDA + U + SO approach, including the Coulomb correlation interaction U and the spin–orbit (SO) coupling. They used a $2 \times 2 \times 1$ anatase unit cell

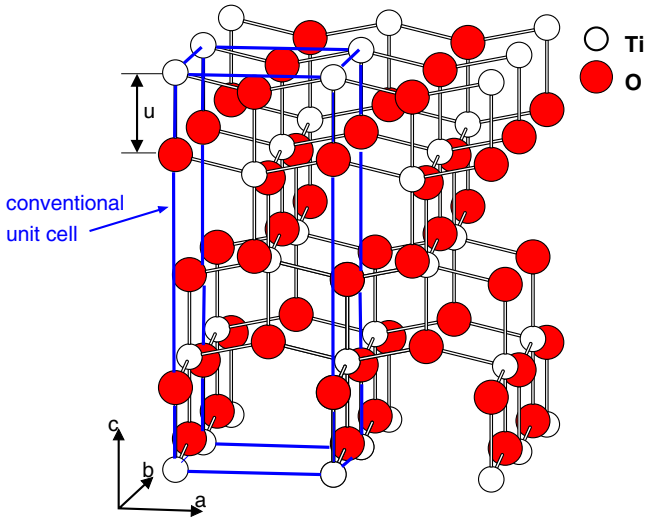

Figure 19. $2 \times 2 \times 1$ anatase supercell as used in most of the calculations performed to date. The conventional body-centred tetragonal unit cell which contains four formula units is indicated.

corresponding to that shown in figure 19 to treat concentrations of substitutional Co impurities of 12.5 and 6.25 at.% respectively (i.e. two or one Ti atom(s) replaced by Co, the latter system being used to study the influence of oxygen vacancies). The unit cell parameters used were the experimental values $a = b = 3.785$ Å, and $c = 9.514$ Å, and the internal displacement parameter was $u = 0.208$.

The two substitutional Co atoms were placed at a distance of 5.353 Å from each other along [110]. LSDA calculations showed that in this configuration a ferromagnetic alignment of the Co magnetic moments is lower in energy than an antiferromagnetic one by $\Delta E \approx 6$ mRyd. Assuming the energy difference between ferromagnetic and antiferromagnetic alignment of magnetic moments to be an upper limit for the exchange energy, one can approximate T_C by setting $\Delta E = k_B T_C$. Using the result of Park *et al* would yield $T_C \approx 950$ K. However, since relaxations of the structure upon substituting Ti by Co were not included in [41], this value should be considered a rough estimate.

Park *et al* reported that the AFM phase exhibited the electronic structure of a semiconductor, while the FM phase was half-metallic with a magnetic moment of 1 μ_B per Co atom. A possible mechanism suggested for explaining the ferromagnetic ground state is a *double-exchange-like* mechanism, i.e. a kinetic energy gain through the hopping of fully spin-polarized carriers in the half-metallic system. But since strictly speaking double exchange requires the presence of mixed valency in the system, this mechanism is better described more generally as carrier-mediated exchange.

The influence of Coulomb correlation interaction and/or the Jahn–Teller interaction on the band structure was investigated using LSDA + U + SO electronic structure calculations, with $U = 3$ eV and $J = 0.87$ eV. The same supercell was used, but with only one substitutional Co atom (corresponding to 6.25 at.%); as a consequence only a ferromagnetic solution was allowed. In contrast to the LSDA solution for the FM phase, a semiconducting ground state was found; such an opening of a gap in an LSDA band structure on application of a U is typical. In addition to the spin magnetic moment, Co now also exhibited an orbital magnetic moment of 0.9 μ_B; a rather high value comparable to that of Co in CoO ($\approx$1.0 μ_B). Thus the total

magnetic moment of Co amounted to 1.9 μ_B. The occurrence of such a large orbital moment in a LDA treatment of this system deserves some attention. On the one hand, including the spin–orbit coupling results in an indirect l–l interaction via the spins, so an orbital moment can be made visible. However, for the given situation—the Fermi level lies at a peak of the density of states—we can also expect that the application of a U of 3 eV lifted any remaining degeneracies between the unoccupied and occupied d states at the Fermi level, suppressing any orbital moment. A more detailed investigation of the orbital and spin moments for a range of different U would be valuable here.

For the investigation of the influence of oxygen vacancies by Park *et al*, the same supercell with 6.25 at.% Co was used. An oxygen atom was first removed from an octahedron containing a Ti atom (A), and next from the octahedron containing the Co atom (B). Total energy LSDA + U + SO calculations showed case A to be more stable. In this case the presence of the vacancy changed neither the spin nor the orbital magnetic moment of the Co atom. In case B, however, the presence of the vacancy seemed to lead to an 'intermediate' spin state, resulting from the altered crystal field, increasing the spin moment to 2.53 μ_B and reducing the orbital magnetic moment to 0.28 μ_B (giving a total magnetic moment of 2.81 μ_B per Co atom). The influence of oxygen vacancies on the stability of the ferromagnetic phase was not evaluated.

Yang *et al* [95] used the full potential linearized augmented plane-wave (FLAPW) method as well as the pseudopotential Cambridge serial total energy package (CASTEP) [149] in the LSDA to investigate the distribution and magnetization of substitutional Co impurities in anatase and rutile TiO_2. Supercells built of $2 \times 2 \times 1$, $2 \times 2 \times 2$, and $4 \times 2 \times 1$ unit cells (48 and 96 atoms respectively) were employed to treat Co concentrations of 12.5 and 6.25 at.%.

The lattice constants calculated with CASTEP were $a = 3.74$ Å and $c = 9.52$ Å for anatase, and $a = 4.59$ Å and $c = 2.95$ Å for rutile, which agree well with experimental values. In the case of pure TiO_2 the anatase structure was calculated to be lower in energy than the rutile one by 18 meV per formula unit, which corresponds to approximately 0.4 kcal mol^{-1} TiO_2. As mentioned in the introduction, generally the rutile phase is considered to be slightly more stable than the anatase; the discrepancy might be the result of the pseudopotential used in the calculation [150].

Doping the structures with one substitutional Co (6.25 at.%) reversed the trend; Co-doped rutile was lower in energy than Co-doped anatase by the surprisingly large value of ≈0.5 eV per TiO_2 formula unit ($\widehat{=}$5.5 kcal mol^{-1}).

The Co-doping (at fixed volume, but with relaxed internal coordinates) only led to a small, local geometrical distortion around the impurity of less than 0.1 Å. Still, the substitution energies were rather high; in the 48-atom supercell, 7.23 eV per Co atom in rutile and 8.51 eV/Co in anatase were obtained. These high defect energies suggest that a segregation of the impurities to surfaces, interfaces, or other defects which provide more free space is likely.

To investigate the influence of the Co distribution on the magnetism in anatase, Yang *et al* tested three different configurations with the FLAPW method: (I) the Co atoms forming a grid in the (001) plane with periodicity $2a$ and grid–grid spacing c (the 'uniform' distribution); (II) a grid in the (001) plane with periodicity $\sqrt{2a}$ and grid–grid spacing c; and (III) chains of Co atoms along [100] with chain–chain distances of $2a$ along [010] and c along [001]. In all cases the ground state was ferromagnetic (note that, in the uniform distribution, there was no other possibility, due to the periodic boundary conditions) with only slight variations in the magnetic moments, which ranged from 0.68 to 0.71 μ_B per Co atom. Configuration (III) was lowest in energy, indicating that a not perfectly homogeneous distribution of Co in anatase TiO_2 is favourable. In this case also a metastable, ferrimagnetic arrangement of the Co spins could be observed, with alternating magnetic moments of −0.44 and +0.88 μ_B

per Co atom. Unfortunately the authors did not investigate the origin of this interesting spin disproportionation further.

In rutile, only the uniform distribution of Co was tested, but with a doubled unit cell, so that an antiferromagnetic arrangement of the Co spins could also be probed. The antiferromagnetic arrangement indeed turned out to be the ground state, in both the FLAPW and CASTEP calculations. The magnetic moments varied from 0.55 (CASTEP) to 0.72 (FLAPW) μ_B per Co. The authors concluded that an inhomogeneous Co distribution is crucial for the observation of ferromagnetism in TiO_2.

Errico *et al* investigated Mn-, Fe-, Co-, and Ni-doped rutile, employing both the LDA and the GGA approximations [45, 69]. They found that the two approximations of the exchange–correlation functional give similar results: a monotonically decreasing magnetic moment per transition metal ion from Mn to Fe to Co to Ni, which was independent of the dopant concentration ($x = 0.0625$, 0.25, and 0.5), and distribution of the ions. Only in the case of Fe doping did the magnetic moment and the nature of the magnetic coupling depend on the relative metal–metal positions. In contrast, Errico *et al* found Co-doped TiO_2 to be *always* ferromagnetic, and Mn-doped rutile to be always antiferromagnetic, independently of the impurity distribution in the host. All the systems except the cell containing Ni were insulating.

5.2.2. More defects. Sullivan and Erwin [42] used density functional theory as implemented in the Vienna *ab initio* Simulation Package (VASP) [151], a plane-wave pseudopotential code, to determine the electronic structure, formation energy, and electrical activity of Co dopants and oxygen vacancies in TiO_2 anatase. The LDA was used for total energy calculations, with systems involving Co atoms treated in a spin-polarized fashion. The authors then employed equilibrium thermodynamics to predict, as a function of temperature, the concentrations of defects in the TiO_2 host over a range of Co and O chemical potentials, corresponding to different experimental growth conditions.

The calculated defect formation energies as a function of the oxygen chemical potential showed that, in the O-rich limit, the substitutional site is favourable for Co, where it forms in a charge neutral form (oxidation state IV, magnetic moment $\mu = 1.0\ \mu_B$). In the O-poor limit, interstitial Co in the +1 and +2 charge states (oxidation state I, $\mu = 2.0\ \mu_B$, and oxidation state II, $\mu = 1.0\ \mu_B$, respectively) becomes energetically competitive with substitutional Co. The concentration of isolated oxygen vacancies, as well as that of complexes of substitutional Co and an oxygen vacancy, remained negligible for all thermodynamically allowed chemical potentials. This indicates that oxygen vacancies should not play any significant role in determining the carrier concentration in Co-doped samples, which is in conflict with e.g. the results of Toyosaki *et al* [17] (for rutile).

The authors stress that neither substitutional nor interstitial Co has any significant orbital moment (in contrast to the indications of the calculations of Park *et al* [41]). Thus they conclude that the experimentally observed magnetic moments larger than 1 μ_B per Co could only result from the statistical distribution of Co moments in interstitial (2 μ_B) and substitutional (1 μ_B) sites, corresponding to *oxygen-poor* growth conditions. In this case the observed n-type conducting behaviour would result from thermal excitation of electrons from interstitial Co into the conduction band.

The influence of interstitial Co on the ferromagnetism in anatase [152] and rutile [44] TiO_2 was also investigated by Geng and Kim. They performed spin-polarized band structure calculations in the generalized gradient approximation (GGA) using VASP. Their supercells consisted of $2 \times 2 \times 1$ TiO_2 unit cells (48 atoms), and substitutional Co concentrations of 6.25 and 12.5 at.% were considered.

The formation energy of interstitial Co (Co^I) as a neutral defect was very high, i.e. $E_f^I = +2.07$ eV. However, having a substitutional Co (Co^S) in its vicinity reduced the formation energy of Co^I to +0.18 eV, and in the case of two neighbouring Co^S, E_f^I was −0.49 eV. So it was concluded that 'clustering' of substitutional Co attracts interstitial Co.

Both Co^S and Co^I were found to be in the low spin state. In a sphere of radius $r = 1.1$ Å around the Co atom, the spin magnetic moments were $\mu^S = 0.73\ \mu_B$ for a single substitutional Co, and $\mu^S = 0.69\ \mu_B$ in the case of two substitutional Co in the supercell. The two substitutional Co atoms were always found to couple ferromagnetically, independently of the Co–Co distance. The case of two substitutional Co with one interstitial atom in their vicinity was particularly interesting, with values of $\mu_1^S = -0.01\ \mu_B$, $\mu_2^S = -0.07\ \mu_B$, and $\mu^I = 1.04\ \mu_B$. This implies that in $2Co^S + Co^I$ complexes the magnetic moments of substitutional and interstitial Co are aligned in a ferrimagnetic fashion, leading to an *average* spin magnetic moment of only $0.32\ \mu_B$/Co. In agreement with Sullivan *et al* [42], Geng and Kim suggest this as a possible explanation for the discrepancy between the high total magnetic moments calculated by Park *et al* [41] (up to 2.9) and the various experimentally measured magnetic moments.

The electronic structure calculated by Geng and Kim was also affected by the presence of interstitial Co. In the LSDA, while TiO_2 doped with substitutional Co exhibited a half-metallic density of states (DOS), the system was metallic when the impurities were interstitials. TiO_2 with a $2Co^S + Co^I$ complex had the DOS of a semiconductor.

5.3. Doped ZnO

Much of the recent activity in transition metal-doped ZnO was motivated by the theoretical prediction [11] that p-type ZnO doped with 5 at.% of Mn should be a room temperature ferromagnet. The prediction was based on a mean field approach, assuming hole-mediated ferromagnetic interactions between the Mn local moments. The Curie temperature was then determined from a competition between this long range carrier-mediated ferromagnetic coupling and short range Mn–Mn antiferromagnetic exchange interactions.

Following this prediction, Sato *et al* [153] used the Korringa–Kohn–Rostoker (KKR) Green function method based on the local density approximation of density functional theory to calculate the properties of ZnO doped with the 3d transition metal ions V, Cr, Mn, Fe, Co, and Ni. $2 \times 2 \times 1$ supercells containing eight formula units of ZnO were used, with two Zn atoms replaced with transition metal atoms, resulting in a doping concentration of 25%. Additional holes were introduced by replacing O with N, while electrons were added by replacing some of the Zn atoms with Ga. The ZnO experimental lattice parameters, $a_0 = 3.27$ Å and $c_0 = 5.26$ Å [154], were adopted for all the calculations. The difference in the energies of the ferromagnetic and the antiferromagnetic ordering was taken as an upper limit to the Curie temperature, T_C. A plot showing the energy difference as a function of the different transition metal ions is shown in figure 20. The ferromagnetic state, with a T_C of around 2000 K, was predicted to be favourable for V, Cr, Fe, Co, and Ni in ZnO while Mn-doped ZnO was antiferromagnetic. The energy difference ($E_{fm} - E_{afm}$) was in the region of 0.2 eV which corresponds to a T_C of about 2000 K. Note that no structural relaxations were performed after substitution of the transition metal ions.

Using the GGA approximation, ultrasoft pseudopotentials and plane-wave basis sets, Cheng and Lee [155] calculated the energy difference between ferromagnetic and antiferromagnetic alignments for two Co atoms substituted in ZnO. Supercells of $2 \times 2 \times 1$, $2 \times 1 \times 2$, and $4 \times 1 \times 1$ were used to allow different Co–Co distances. For a Co doping level of 25% in a $2 \times 2 \times 1$ supercell, two different cases were investigated: one in which the two

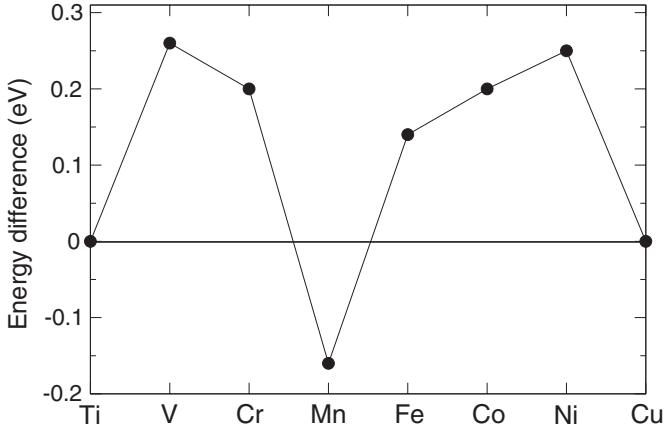

Figure 20. Energy difference ($E_{\mathrm{afm}} - E_{\mathrm{fm}}$) for the 3d transition metal ion dopants in ZnO. Data taken from [153].

Co atoms were aligned along the basal plane and the other in which they were aligned along the *c* axis. In the former case, the AFM state was found to be more stable by about 34 meV per Co atom than the FM state, while in the latter, the FM was lower in energy by about 1 meV per Co atom. To find the range of AFM interactions between Co atoms, different geometries were tested for a Co pair in a supercell, increasing the Co–Co distance in three steps from 3.28 to 6.56 Å. In all cases, the total energy difference between the FM and the AFM states was less than 3 meV per Co atom. The results indicated that the couplings between two Co ions are negligible for distances larger than 4.6 Å, and suggested that the range of magnetic interactions is short. The authors also investigated the effect of electron doping at the level of one electron per Co atom and found that the FM state is more stable by 94 and 69 meV per Co atom for the alignments along the basal plane and the *c*-axis directions, respectively. The main conclusions were: (i) spontaneous magnetization is not possible in intrinsic Co-doped ZnO, (ii) the FM coupling is short ranged and (iii) a high concentration of both Co ions and electron carriers are needed to achieve ferromagnetism.

The effects of doping ZnO with Co and Mn with 6.25% and 12.5% dopant concentration were investigated by Spaldin [156]. DFT/LSDA calculations were performed for 32-atom supercells containing two dopant ions in different positional arrangements: the 'close' configuration in which the TM atoms were separated by a single O ion; and the 'separated' configuration, in which they were connected by an –O–Zn–O– bond. For each of the spatial configurations, the energy difference between the FM and the AFM spin orderings was calculated. For Mn- and Co-doped ZnO, the energy difference between the AFM and the FM was very small: a few meV. Therefore paramagnetic behaviour was predicted for both systems in the absence of free carriers. Holes were introduced by creating Zn vacancies (not easy experimentally); for both Co- and Mn-doped ZnO the FM state was then stabilized. Feng *et al* [157] repeated the calculations for the Mn-doped system using the B3LYP energy functional [158]. They obtained an antiferromagnetic state 'close' case (which they also found to be more energetically favourable than the 'far' configuration) and a FM state, stable by only about 0.01 eV, in the 'far' case. Note that, in both [157] and [156], the positions of the atoms were fixed to the positions of experimental ZnO. However, the effect of relaxations on the magnetic interactions can be large, and generally leads to a decreased energy difference between FM and AFM ordering, as discussed in [159].

In summary, most electronic structure computations published to date agree that intrinsic ferromagnetism does not occur in doped ZnO at reasonable doping concentrations, but in many cases the addition of carriers stabilizes the ferromagnetic state. Most published reports, however, have not included full atomic relaxations on addition of the magnetic ions [153, 156, 157].

Finally we note that there is also a large activity in the area of mean field descriptions based on Kohn–Luttinger model Hamiltonians, especially for III–V-based systems (e.g. [160, 161]), but also for tetrahedral hosts in general, including ZnO (see e.g. [162]). This line of work is beyond the scope of this review.

6. Discussion and conclusions

6.1. Transition metal-doped TiO_2

Although the variety of computational and experimental results is at first glance confusing, some general rules can be extracted from our literature review. For example it is clear that $LaAlO_3$ is always a good substrate for obtaining the anatase structure. In combination with very low growth rates (when MBE is employed) one obtains epitaxial samples with a homogeneous Co distribution [16, 19]. Assuming a homogeneous distribution of Co on substitutional sites, both calculations and experiment show that Co-doped TiO_2 anatase is a ferromagnet, with experiments suggesting critical temperatures of about 650 K. However, obtaining such a homogeneous distribution is an experimentally very demanding task.

Furthermore the reported values for the magnetic moment per Co atom scatter over a wide range in experimental as well as computational investigations. Calculations suggest that the measured magnetic moments could result from complexes of interstitial and substitutional Co; however, experiments in general do not show signs of interstitial Co. Thus the exact value of the magnetic moment per Co atom remains unclear. The observation of metallic inclusions in many experimental samples suggests, however, that very high saturation magnetizations (1.7 μ_B per Co atom and higher) are not due to intrinsic ferromagnetism but possibly result from the presence of superparamagnetic particles.

When a homogeneous Co distribution is achieved, there is experimental evidence that the ferromagnetism is carrier mediated [19], which is supported by the calculated (in the LSDA) half-metallic DOS [41], and the fact that FM coupling does not seem to depend on the Co–Co distance [152]. However, the half-metallic density of states obtained by LSDA calculations is not likely to persist if a beyond-LDA method is used [41]. Thus, more detailed computational analyses of the electronic structure with methods that include correlation effects are badly needed to determine the origin of the ferromagnetism and to explain the very high Curie temperatures.

An interesting model, originally proposed to explain the ferromagnetism in substituted zinc oxide, is that of Venkatesan and Coey [49], who propose that high Curie temperatures are found whenever the impurity band overlaps unoccupied 3d states of the host oxide. According to the calculations discussed in this review [41, 42, 44, 152] this is not the case for ideal $Co_xTi_{1-x}O_2$, in which the Co impurity states are centred in the band gap. However, the impurity states are shifted towards the conduction band in the presence of oxygen vacancies [163], which could enable this mechanism. Apart from this fact, however, the influence of oxygen vacancies on the magnetic moment or magnetic interaction in TiO_2 is unclear, with theory and experiment providing contradictory results [17, 42]. Clearly further work is needed in this area.

According to [30], oxygen vacancies could enhance Co mobility and therefore increase clustering. As mentioned before, experimental investigations in general show a tendency of

Co to segregate to interfaces or precipitates, or to cluster, leading to enriched regions or even metallic, superparamagnetic particles. This can partly be understood from the high defect energies of Co in TiO_2 [44, 152] and shows that great care has to be applied in sample growth and characterization. A strong influence of segregation and the presence of enriched regions on the magnetic properties is evident, but the origins are not yet perfectly clear and further work in this area is desirable. For example, there is evidence that internal interfaces such as grain boundaries not only give direction to segregation but also can change the sign of the magnetic interaction [164].

The computational part of this review suffers from the small number of studies of Co-doped TiO_2, and the fact that slightly different methods are used in all cases. Here comparative studies with different LDA and 'beyond-LDA' methods, as well as extensive studies of the convergence parameters of the different approaches, will be helpful.

Finally we suggest some guidelines for producing robust room temperature ferromagnetic Co-doped TiO_2, with well-defined properties and high saturation magnetization.

A homogeneous Co distribution seems to be the most important factor. Samples with inhomogeneous distributions do exhibit room temperature ferromagnetism, but Co is likely to cluster, leading to non-reproducible properties, that are not desirable:

- small 'clusters' (2–3 atoms) of Co atoms have an average magnetic moment much smaller than that of an isolated atom;
- large, metallic Co particles have high total magnetic moments, but they show superparamagnetic behaviour with size-dependent switching fields, and furthermore they tend to destroy the semiconducting properties of the host oxide.

To achieve a homogeneous distribution, the Co concentration should not exceed 10 at.%. Furthermore, since Co shows a strong tendency to segregate to any kind of structural defect, the TiO_2 host material should be perfectly epitaxial. For anatase, this is best achieved on a $LaAlO_3$ substrate and at very low growth rates ($\leqslant 0.03$ Å s^{-1}).

The oxygen partial pressure is a factor that has to be further investigated, since on the one hand the presence of O vacancies probably promotes ferromagnetic coupling, but on the other hand it also enhances Co segregation.

The above-mentioned strategies still cannot guarantee the production of an intrinsic DMS; thus the samples obtained should be thoroughly characterized, *ideally* in all of the following ways:

- the structure should be characterized by XRD *and* HRTEM to ensure that it is epitaxial and there are no Co or second phase particles;
- the saturation magnetization should be recorded over a large range of temperatures, especially going to very low temperatures, to identify blocked behaviour resulting from the presence of small superparamagnetic particles that are not visible in HRTEM;
- T_C should actually be determined (instead of just giving a lower boundary); T_C will also be valuable as an input or test value for models describing the underlying mechanism of the ferromagnetism.

The data for other transition metal dopants in TiO_2 are still sparse, but we can say that doping TiO_2 with iron seems to be even more difficult than doping it with Co, due to the strong tendency of Fe to form second phases [71]. Cr, on the other hand, seems to distribute more easily in a homogeneous fashion [65]. As regards high saturation magnetizations, vanadium seems to be a promising candidate [28]; however, the origin of the large measured moments is still unclear.

6.2. Transition metal-doped ZnO

In spite of the early promise predicted for ferromagnetism in ZnO-based magnetic semiconductors [11], many difficulties remain. In experimental studies, as in the case of TiO_2, choosing the right growth conditions is important. Low growth temperatures, high oxygen pressure, and dilute concentrations of transition metal ions lead to a homogeneous distribution of the transition metal dopants, and weaken the AFM exchange to favour FM interactions. The experimentally observed tendency of precipitation of second phases at higher concentrations, and the decreasing saturation magnetization for Mn-doped samples with increasing concentration are particularly challenging practical issues. A comparison of thin film and bulk studies suggests that many reports of magnetism might not be intrinsic. And the presence of carriers, particularly holes, seems to be crucial in many cases for the mediation of ferromagnetic interactions. As in the case of TiO_2-based thin films, a clearer understanding of the experimental situation will only be obtained when thorough characterizations are performed before interpreting the results.

In the computational studies, care needs to be taken to optimize the structure after the transition metal ions are introduced, since relaxations of the atomic positions can drastically reduce the energy differences of interest, or even change the sign. Again, evaluating the LDA results in the light of more beyond-LDA studies is desirable. Mean field studies of tetrahedrally coordinated semiconductors indicate that in doped ZnO the effect of spin–orbit coupling is important (see e.g. [103]); thus it could be essential to include this in the *ab initio* calculations, too.

Acknowledgments

The authors thank James Sullivan and Ram Seshadri for helpful discussions. This work was supported by the National Science Foundation's Information Technology Research programme through the Division of Materials Research, grant number DMR-0312407 (RJ), and the Department of Energy, grant number DE-FG03-02ER45986 (PG). Furthermore we made use of MRL facilities, supported by the MRSEC programme of the National Science Foundation under award No DMR00-80034.

References

[1] Das Sarma S 2001 *Am. Sci.* **89** 516
[2] Feynman R P 1986 *Found. Phys.* **16** 507
[3] Mauger A and Godart C 1986 *Phys. Rep.* **141** 51
[4] Treitinger L, Göbel H and Pink H 1976 *Mater. Res. Bull.* **11** 1375
[5] Steigmeier E and Harbeke G 1970 *Phys. Kondens. Mater.* **12** 1
[6] Furdyna J 1988 *J. Appl. Phys.* **64** R29
[7] Haury A, Wasiela A, Arnoult A, Cibert J, Tatarenko S, Dietl T and Merle d'Aubigné Y 1997 *Phys. Rev. Lett.* **79** 511
[8] Ohno H 1998 *Science* **281** 951
[9] Sanvito S, Theurich G and Hill N A 2002 *J. Supercond.* **15** 85
[10] Matsumoto Y, Murakami M, Shono T, Hasegawa T, Fukumura T, Kawasaki M, Ahmet P, Chikyow T, Koshihara S and Koinuma H 2001 *Science* **291** 854
[11] Dietl T, Ohno H, Matsukura F, Cibert J and Ferrand D 2000 *Science* **287** 1019
[12] Sharma P, Gupta A, Rao K, Owens F J, Sharma R, Ahuja R, Osorio-Guillen J, Johansson B and Gehring G 2003 *Nat. Mater.* **2** 673
[13] Theodoropoulou N, Misra V, Philip J, LeClair P, Berera G P, Moodera J S, Satpati B and Som T 2004 *Preprint* cond-mat/0408294
[14] Lim S W, Jeong M C, Ham M H and Myoung J M 2004 *Japan. J. Appl. Phys.* **43** L280
[15] Kolesnik S, Dabrowski B and Mais J 2004 *J. Appl. Phys.* **95** 2582
[16] Kim J-Y *et al* 2003 *Phys. Rev. Lett.* **90** 017401

[17] Toyosaki H, Fukumura T, Yamada Y, Nakajima K, Chikyow T, Hasegawa T, Koinuma H and Kawasaki M 2004 *Nature* **3** 221
[18] Chambers S A *et al* 2001 *Appl. Phys. Lett.* **79** 3467
[19] Chambers S A, Wang C M, Thevuthasan S, Droubay T, McCready D E, Lea A S, Shutthanandan V and Windisch C F Jr 2002 *Thin Solid Films* **418** 197
[20] Chambers S A, Droubay T, Wang C M, Lea A S, Farrow R F C, Folks L, Deline V and Anders S 2003 *Appl. Phys. Lett.* **82** 1257
[21] Fukumura T *et al* 2003 *Japan. J. Appl. Phys.* **42** L105
[22] Shinde S R *et al* 2003 *Phys. Rev.* B **67** 115211
[23] Stampe P, Kennedy R, Xin Y and Parker J 2003 *J. Appl. Phys.* **93** 7864
[24] Higgins J S, Shinde S R, Ogale S B, Venkatesan T and Greene R L 2004 *Phys. Rev.* B **69** 073201
[25] Park W, Ortega-Hertogs R, Moodera J, Punnoose A and Seehra M 2002 *J. Appl. Phys.* **91** 8093
[26] Balagurov L, Klimonsky S, Kobeleva S, Orlov A, Perov N and Yarkin D 2004 *JETP Lett.* **79** 98
[27] Yang H and Singh R 2004 *J. Appl. Phys.* **95** 7192
[28] Hong N, Prellier W, Sakai J and Ruyter A 2004 *J. Appl. Phys.* **95** 7378
[29] Yao X, Zhou T, Gai Y, Chong T and Wang J 2004 *J. Appl. Phys.* **95** 7375
[30] Kim D *et al* 2002 *Appl. Phys. Lett.* **81** 2421
[31] Shinde S R, Ogale S B, Higgins J S, Zheng H, Millis A J, Kulkarni V N, Ramesh R, Greene R L and Venkatesan T 2004 *Phys. Rev. Lett.* **92** 166601
[32] Kim D, Yang J, Kim Y, Chang Y, Noh T, Bu S, Kim Y-W, Park Y, Pearton S and Park J-H 2004 *Ann. Phys.* **13** 70
[33] Kennedy R, Stampe P, Hu E, Xion P, von Molár S and Xin Y 2004 *Appl. Phys. Lett.* **84** 2832
[34] Cui M, Zhu J, Zhong X, Zhao Y and Duan X 2004 *Appl. Phys. Lett.* **85** 1698
[35] Shutthanandan V *et al* 2004 *Appl. Phys. Lett.* **84** 4466
[36] Manivannan A, Glaspell G and Seehra M 2003 *J. Appl. Phys.* **94** 6994
[37] Yamade Y *et al* 2004 *J. Appl. Phys.* **96** 5097
[38] Kim D *et al* 2005 *Phys. Rev.* B **71** 014440
[39] Khaibullin R, Tagirov L, Rameev B, Ibragimov S, Yildiz F and Aktaş B 2004 *J. Phys.: Condens. Matter* **16** L443
[40] Joh Y G, Kim H D, Kim B Y, Woo S J, Moon S H, Cho J H, Kim E C, Kim D H and Cho C R 2004 *J. Korean Phys. Soc.* **44** 360
[41] Park M, Kwon S and Min B 2002 *Phys. Rev.* B **65** 161201
[42] Sullivan J M and Erwin S C 2003 *Phys. Rev.* B **67** 144415
[43] Geng W T and Kim S K 2004 *Solid State Commun.* **129** 741
[44] Geng W T and Kim S K 2003 *Phys. Rev.* B **68** 125203
[45] Errico L, Weissmann M and Rentería M 2004 *Phys. Status Solidi* b **241** 2399
[46] Zheng Y, Bouilliard J C, Demaille D, Bernard Y and Petroff J F 2005 *J. Cryst. Growth* **274** 156
[47] Ueda K, Tabata H and Kawai T 2001 *Appl. Phys. Lett.* **79** 988
[48] Jin Z *et al* 2001 *Appl. Phys. Lett.* **78** 3824
[49] Venkatesan M, Fitzgerald C B, Lunney J G and Coey J M D 2004 *Phys. Rev. Lett.* **93** 177206
[50] Kim J H, Kim H, Kim D, Ihm Y E and Choo W K 2002 *J. Appl. Phys.* **92** 6066
[51] Kim J H, Kim H, Kim D, Ihm Y E and Choo W K 2003 *Physica* B **327** 304
[52] Prellier W, Fouchet A, Mercey B, Simon C and Raveau B 2003 *Appl. Phys. Lett.* **82** 3490
[53] Yoo Y-Z, Fukumura T, Jin Z, Hasagewa K, Kawasaki M, Ahmet P, Chikyow T and Koinuma H 2001 *J. Appl. Phys.* **90** 4246
[54] Rode K, Anane A, Mattana R, Contour J-P, Durand O and LeBourgeouis R 2003 *J. Appl. Phys.* **93** 7676
[55] Yan L, Ong C K and Rao X S 2004 *J. Appl. Phys.* **96** 508
[56] Ramachandran S, Tiwari A and Narayan J 2004 *Appl. Phys. Lett.* **84** 5255
[57] Lim S W, Hwang S K and Myoung J M 2003 *Solid State Commun.* **125** 231
[58] Yang S G, Pakhomov A B, Hung S T and Wong C Y 2002 *IEEE Trans. Magn.* **38** 2877
[59] Lee H J, Jeong S Y, Cho C R and Park C H 2002 *Appl. Phys. Lett.* **81** 4020
[60] Rao C N R and Deepak F L 2005 *J. Mater. Chem.* **15** 573
[61] Hong N, Prellier W, Sakai J and Ruyter A 2005 *Physica* B **355** 295
[62] Saeki H, Tabata H and Kawai T 2001 *Solid State Commun.* **120** 439
[63] Saeki H, Matsui H, Kawai T and Tabata H 2004 *J. Phys. Chem.* **16** S5533
[64] Hong N, Ruyter A, Prellier W and Sakai J 2004 *Appl. Phys. Lett.* **85** 6212
[65] Droubay T, Heald S, Shutthanandan V, Thevuthasan S and Chambers S 2005 *J. Appl. Phys.* **97** 046103

[66] Wang Z, Tang J, Zhang H, Golub V, Spinu L and Tung L 2004 *J. Appl. Phys.* **95** 7381
[67] Lee H J, Jeong S Y, Hwang J Y and Cho C R 2003 *Europhys. Lett.* **64** 797
[68] Park M and Min B 2003 *Phys. Rev.* B **68** 033202
[69] Errico L, Weissmann M and Rentería M 2004 *Physica* B **354** 338
[70] Wang Z, Wang W, Tang J, Tung L, Spinu L and Zhou W 2003 *Appl. Phys. Lett.* **83** 518
[71] Kim Y, Thevuthasan S, Droubay T, Lea A, Wang C, Shutthanandan V, Chambers S, Sears R, Taylor B and Sinkovic B 2004 *Appl. Phys. Lett.* **84** 3531
[72] Kim E, Moon S, Woo S, Cho J, Joh Y and Kim D 2004 *Solid State Commun.* **132** 477
[73] Hong N, Prellier W, Sakai J and Hassini A 2004 *Appl. Phys. Lett.* **84** 2850
[74] Hong N, Sakai J and Prellier W 2004 *J. Magn. Magn. Mater.* **281** 347
[75] Hong N, Sakai J and Prellier W 2004 *Phys. Rev.* B **70** 195204
[76] Cho Y M, Choo W K, Kim H, Kim D and Ihm Y 2002 *Appl. Phys. Lett.* **80** 3358
[77] Wakano T, Fujimura N, Morinaga Y, Abe N, Ashida A and Ito T 2001 *Physica* E **10** 260
[78] Anderson P W 1963 *Magnetism* ed G Rado and H Suhl (New York: Academic) chapter 2, p 25
[79] White R 1983 *Quantum Theory of Magnetism* (Berlin: Springer)
[80] Yosida K 1996 *Theory of Magnetism* (Berlin: Springer)
[81] Zener C 1951 *Phys. Rev.* **81** 440
[82] Zener C 1951 *Phys. Rev.* **83** 299
[83] Zener C 1951 *Phys. Rev.* **82** 403
[84] Torrance J, Shafer M and McGuire T 1972 *Phys. Rev. Lett.* **29** 1168
[85] Durst A, Bhatt R and Wolff P 2002 *Phys. Rev.* B **65** 235205
[86] Angelescu D and Bhatt R 2002 *Phys. Rev.* B **65** 075221
[87] Kübler J and Vigren D 1975 *Phys. Rev.* B **11** 4440
[88] Muscat J, Swamy V and Harrison N 2002 *Phys. Rev.* B **65** 224112
[89] Calatayud M, Mori-Sánchez P, Beltrán A, Pendás A, Francisco E, Andrés J and Recio J 2001 *Phys. Rev.* B **64** 184113
[90] Ranade M, Navrotsky A, Zhang H, Banfield J, Elder S, Zaban A, Borse P, Kulkarni S, Doran G and Whitfield H 2002 *Proc. Natl Acad. Sci. USA* **99** 6476
[91] Banfield J, Bischoff B and Anderson M 1993 *Chem. Geol.* **110** 211
[92] Hagfeldt A and Grätzel M 2000 *Acc. Chem. Res.* **33** 269
[93] Murakami M, Matsumoto Y, Hasegawa T, Ahmet P, Nakajima K, Chikyow T, Ofuchi H, Nakai I and Koinuma H 2004 *J. Appl. Phys.* **95** 5330
[94] Matsumoto Y, Murakami M, Jin Z, Ohtomo A, Lippmaa M, Kawasaki M and Koinuma H 1999 *Japan. J. Appl. Phys.* **38** L603
[95] Yang H, Choi J, Craciun V and Singh R 2003 *J. Appl. Phys.* **93** 7873
[96] Lewis B and Anderson J 1978 *Nucleation and Growth of Thin Films* (New York: Academic)
[97] Aleksandrov L 1984 *Growth of Crystalline Semiconductor Materials on Crystal Surfaces* (Amsterdam: Elsevier)
[98] Reimer L 1989 *Transmission Electron Microscopy: Physics of Image Formation and Microanalysis* (Berlin: Springer)
[99] Kuzmany H 1998 *Solid-State Spectroscopy: an Introduction* (New York: Springer)
[100] Nalwa H 2002 *Handbook of Thin Film Materials* (San Diego, CA: Academic)
[101] Suryanarayanan R, Naik V, Kharel P, Talagala P and Naik R 2005 *Solid State Commun.* **133** 439
[102] Suryanarayanan R, Naik V, Kharel P, Talagala P and Naik R 2005 *J. Phys.: Condens. Matter* **133** 439
[103] Dietl T and Ohno H 2003 *MRS Bull.* (October) 714
[104] Morrish A 1965 *The Physical Principles of Magnetism* (New York: Wiley)
[105] Makino T, Segawa Y, Kawasaki M, Ohtomo A, Shoroki R, Tamura K, Yasuda T and Koinuma H 2001 *Appl. Phys. Lett.* **78** 1237
[106] Ohtomo A, Kawasaki M, Koida T, Masubuchi K, Koinuma H, Sakurai Y, Yoshida Y, Yasuda T and Yoshida Y 1998 *Appl. Phys. Lett.* **72** 2466
[107] Wood V E and Austin A E 1975 *Magnetoelectric Interaction Phenomena in Crystals* (London: Gordon and Breach)
[108] Ahmin A 1989 *J. Am. Ceram. Soc.* **72** 369
[109] Fukumura T, Jin Z and Kawasaki M 2001 *Appl. Phys. Lett.* **78** 958
[110] Mizokawa T, Nambu T, Fujimori A, Fukumura T and Kawasaki M 2002 *Phys. Rev.* B. **65** 085209
[111] Tiwari A, Jin C, Kwit A, Kumar D, Muth J F and Narayan J 2002 *Solid State Commun.* **121** 371
[112] Savchuk A I, Gorley P N, Khomyak V V, Ulyanytsky K S, Bilichuk S V, Perrone A and Nikitin P I 2004 *Mater. Sci. Eng.* B **109** 196

[113] Kim Y M, Yoon M, Park I W, Park Y J and Lyou J H 2004 *Solid State Commun.* **129** 175
[114] Cheng X M and Chien C 2003 *J. Appl. Phys.* **93** 7876
[115] Kim D S, Lee S, Min C, Kim H M, Yuldasheva U, Kang T W, Kim D Y and Kim T W 2003 *Japan. J. Appl. Phys.* **42** 7217
[116] Heo Y W, Ivill M P, Ip K, Norton D P, Pearton S J, Kelly J G, Rairigh R, Hebard A F and Steiner T 2004 *Appl. Phys. Lett.* **84** 2292
[117] Bates C H, White W B and Roy R 1966 *J. Inorg. Nucl. Chem.* **28** 397
[118] Jung S W, An S-J, Yi G, Jung C, Lee S and Cho S 2002 *Appl. Phys. Lett.* **80** 4561
[119] Kundaliya D *et al* 2004 *Nat. Mater.* **3** 709
[120] Kim J H, Choo W K, Kim H, Kim D and Ihm Y E 2003 *J. Korean Phys. Soc.* **42** S258
[121] Park J H, Kim M G, Jang H M, Ryu S and Kim Y M 2004 *Appl. Phys. Lett.* **84** 1338
[122] Yin Z, Chen N, Chai C and Yang F 2004 *J. Appl. Phys.* **96** 5093
[123] Lawes G, Risbud A S, Ramirez A P and Seshadri R 2005 *Phys. Rev.* B **71** 045201
[124] Han S J, Lee B Y, Ku J S, Kim Y B and Jeong Y H 2004 *J. Magn. Magn. Mater.* **272** 2008
[125] Kolesnik S, Dabrowski B and Mais J 2002 *J. Supercond.* **15** 251
[126] Roy V A L, Djurišić A B, Liu H, Zhang X X, Leung Y H, Xie M H, Gao J, Lui H F and Surya C 2004 *Appl. Phys. Lett.* **84** 756
[127] Deka S, Pasricha R and Joy P 2004 *Chem. Mater.* **16** 1168
[128] Norton D P *et al* 2003 *Appl. Phys. Lett.* **83** 5488
[129] Kane M H, Shalini K, Summers C J, Varatharajan R, Nause J, Vestal C R, Zhang Z J and Ferguson I T 2005 *J. Appl. Phys.* **97** 023906
[130] Han S J, Jang T H, Kim Y B, Park B G, Park J H and Jeong Y H 2003 *Appl. Phys. Lett.* **83** 920
[131] Theodoropoulou N A *et al* 2003 *Solid State Electron.* **47** 2231
[132] Blythe H J, Ibrahim R M, Gehring G A, Neal J R and Fox A M 2004 *J. Magn. Magn. Mater.* **283** 117
[133] Yoon S W, Cho S B, We S C, Yoon S, Suh B J, Song H K and Shin Y J 2003 *J. Appl. Phys.* **93** 7879
[134] Risbud A S, Spaldin N A, Chen Z Q, Stemmer S and Seshadri R 2003 *Phys. Rev.* B **68** 205202
[135] Lin H, Chin T, Shih J, Lin S, Hong T, Huang R, Chen F and Kai J 2004 *Appl. Phys. Lett.* **85** 621
[136] Lin H, Chin T, Shih J, Huang R, Chen F and Kai J 2004 *Phys. Status Solidi* c **1** 3472
[137] Han S J, Song J W, Yang C H, Park S H, Park J H, Jeong Y H and Rhie K W 2002 *Appl. Phys. Lett.* **81** 4212
[138] Hohenberg P and Kohn W 1964 *Phys. Rev.* **136** B864
[139] Kohn W and Sham L J 1965 *Phys. Rev.* **140** A1133
[140] von Barth U and Hedin L 1972 *J. Phys. C: Solid State Phys.* **5** 1629
[141] Anisimov V, Aryasetiawan F and Lichtenstein A 1997 *J. Phys.: Condens. Matter* **9** 767
[142] Perdew J P and Zunger A 1981 *Phys. Rev.* B **23** 5048
[143] Vogel D, Krüger P and Pollmann J 1998 *Phys. Rev.* B **58** 3865
[144] Svane A, Temmerman W, Szotek Z, Petit L, Strange P and Winter H 2000 *Phys. Rev.* B **62** 13394
[145] Filippetti A and Spaldin N A 2003 *Phys. Rev.* B **67** 125109
[146] Langreth D C and Perdew J P 1980 *Phys. Rev.* B **21** 5469
[147] Langreth D C and Mehl M 1983 *Phys. Rev.* B **28** 1809
[148] Langreth D C and Mehl M J 1984 *Phys. Rev.* B **29** 2310
[149] http://www.tcm.phy.cam.ac.uk/castep
[150] Mikami M, Nakamura S, Kitao O, Arakawa H and Gonze X 2000 *Japan. J. Appl. Phys.* **39** L847
[151] Kresse G and Furthmüller J 1996 *Phys. Rev.* B **61** 11169
[152] Geng W T and Kim S K 2003 *Preprint* cond-mat/0306389
[153] Sato K and Katayuma-Yoshida H 2000 *Japan. J. Appl. Phys.* **39** 555
[154] Mollwo E 1982 *Semiconductors: Physics of II–VI and I–VII Compounds, Semimagnetic Semiconductors* (Berlin: Springer)
[155] Lee E and Chang K J 2004 *Phys. Rev.* B **69** 085205
[156] Spaldin N A 2004 *Phys. Rev.* B **69** 125201
[157] Feng X 2004 *J. Phys. Chem.* **16** 4251
[158] Becke A D 1993 *J. Chem. Phys.* **98** 5648
[159] Spaldin N A and Gopal P 2005 in preparation
[160] Abolfath M, Jungwirth T and MacDonald A 2001 *Physica* E **10** 161
[161] Rodrigues S, Scolfaro L, Leite J, da Cunha Lima I, Sipahi G and Boselli M 2004 *Phys. Rev.* B **70** 165308
[162] Dietl T, Ohno H and Matsukura F 2001 *Phys. Rev.* B **63** 195205
[163] Janisch R and Spaldin N A 2005 in preparation
[164] Janisch R, Gemming S and Spaldin N A 2005 in preparation
[165] Horn M and Schwerdtfeger C 1972 *Z. Kristallogr.* **136** 273
[166] Gemming S and Schreiber M 2005 unpublished